

UNCLASSIFIED

AD NUMBER

AD896220

CLASSIFICATION CHANGES

TO: unclassified

FROM: restricted

LIMITATION CHANGES

TO:
Approved for public release, distribution unlimited

FROM:
Distribution authorized to U.S. Gov't. agencies and their contractors; Administrative/Operational Use; 14 JUL 1952. Other requests shall be referred to Naval Proving Ground, Dahlgren, VA.

AUTHORITY

E.O. 10501, 5 Nov 1953; USNWC ltr, 14 Aug 1975

THIS PAGE IS UNCLASSIFIED

**THIS REPORT HAS BEEN DELIMITED
AND CLEARED FOR PUBLIC RELEASE
UNDER LOJ DIRECTIVE 5200.20 AND
NO RESTRICTIONS ARE IMPOSED UPON
I 'S USE AND DISCLOSURE.**

DISTRIBUTION STATEMENT A

**APPROVED FOR PUBLIC RELEASE;
DISTRIBUTION UNLIMITED.**

UNANNOUNCED

~~SECRET~~

UNCLASSIFIED

2

AD 896220

AD No. _____
DDC FILE COPY

UNANNOUNCED

U. S. NAVAL PROVING GROUND
DAHLGREN, VIRGINIA

REC 2

REPORT NO. 954

THE FOUNDATIONAL RESEARCH PROGRAM
OF THE NAVAL PROVING GROUND

3rd Partial Report

ANALYTICAL SUMMARY PART V PLASTIC FLOW
IN BARS AND SHELLS

FINAL Report

Copy No. _____

Classification _____
SECURITY INFORMATION

DDC
RECEIVED
AUG 9 1952
REGISTERED

LIBRARY OF CONGRESS
REFERENCE DEPARTMENT
TECHNICAL INFORMATION DIVISION
FORMERLY
RESEARCH SECTION

JUL 20 1952
JUL 20 1952

UNCLASSIFIED

~~SECRET~~
~~SECRET~~

UNCLASSIFIED

NPG REPORT NO. 954

Analytical Summary Part V Plastic flow in bars and shells

PART A

SYNOPSIS

↓

An analysis is made of elastic and plastic equilibria in a triangular sheet and in a cylindrical shell. The published data on the deformation and fracture of bars and tubes are reviewed and summarized. Stress-strain diagrams and deformation contours have been obtained on tension and compression specimens of the steel in 37mm PP Type T21 projectiles. The von Karman theory for the propagation of plastic waves in bars is reviewed. The role of the rotation of the axes of strain rate, and the appearance of irrotational flow are analysed. Deformation contours, stream lines and contours of equal velocity potential are given for the irrotational flow in a bar or jet. A few 37mm PP Type T21 projectiles have been fired at an unyielding plate. An analysis is made of the plastic flow and fracture in the projectiles, as revealed by sectioning and etching.

↑

UNCLASSIFIED

UNCLASSIFIED

Analytical Summary Part V Plastic flow in bars and shells

TABLE OF CONTENTS

	Page
SYNOPSIS	1
TABLE OF CONTENTS	2
FOREWORD	3
AUTHORITY	6
OBJECT	6
INTRODUCTION	7
PLASTIC EQUILIBRIUM	9
The plastic deformation of a triangular sheet at equilibrium	
The plastic deformation of a cylindrical shell at equilibrium	
The plastic deformation of a hood at equilibrium	
The static deformation of bars and tubes of mild steel	
PLASTIC FLOW	24
The impact compression of a cylindrical bar	
Plastic flow in cylindrical projectiles	
APPENDIX A - TABLES OF FUNCTIONS	TABLES I-IX (Incl)
APPENDIX B - LIST OF SYMBOLS	1-3 (Incl)
APPENDIX C - BIBLIOGRAPHY	1-2 (Incl)
APPENDIX D - SET OF FIGURES	FIGURES 1-11 (Incl)
APPENDIX E - DISTRIBUTION	1 (Only)

RESTRICTED

NPG REPORT NO. 954

Analytical Summary Part V Plastic flow in bars and shells

FOREWORD

The material in this report has been prepared since World War II in connection with a study of the mechanisms of penetration of plate by projectiles. The report is one of a series of reports. Five of the reports were published at the end of the war, and it was originally planned that nine reports would be submitted altogether. The remaining four reports were held up pending a reevaluation of the ballistic data, inasmuch as there was an opportunity to obtain a few additional tests of special interest at the end of the war. As a result of these tests, the number of reports has been increased to eleven. The six remaining reports are now to be published, but with a minimum expenditure of additional effort in order to bring forth the existing material. The analysis has probably been carried as far as it should be carried without the aid of a modern calculator such as the Mark III Aiken Electronic Calculator. The press of urgent work has thus far prevented allocation of any Mark III time to this work.

RESTRICTED
SECURITY INFORMATION

RESTRICTED

NPG REPORT NO. 954

Analytical Summary Part V Plastic flow in bars and shells

The titles of the full set of eleven reports are as follows:

- (1) ANALYTICAL SUMMARY. PART I. THE PHYSICAL PROPERTIES OF STS UNDER TRIAXIAL STRESS. NPG Report No. 6-46

Object: To summarize the available data on the physical properties of Class B Armor and STS under triaxial stress.

- (2) ANALYTICAL SUMMARY. PART II. ELASTIC AND PLASTIC UNDULATIONS IN ARMOR PLATE. NPG Report No. 7-46

Object: To analyse the propagation of undulations in armor plate; to summarize previous analytical work and to add new analytical work where required in order to complete the theory for ballistic applications.

- (3) ANALYTICAL SUMMARY. PART III. PLASTIC FLOW IN ARMOR PLATE. NPG Report No. 864

Object: To analyse the plastic flow in armor plate adjacent to the point of impact by a projectile.

- (4) ANALYTICAL SUMMARY. PART IV. THE THEORY OF ARMOR PENETRATION. NPG Report No. 9-46

Object: To summarize the theory of armor penetration in its present state of development, and to develop theoretical functions which can be used as a guide in the interpretation of ballistic data.

- (5) ANALYTICAL SUMMARY. PART V. PLASTIC FLOW IN BARS AND SHELLS. NPG Report No. 954

Object: To analyse the plastic flow in cylindrical bars and shells during impact against an unyielding plate.

- (6) ANALYTICAL SUMMARY. PART VI. THE THEORY OF PROJECTILE RICOCHET. (In preparation.)

Object: To analyse the dynamics of projectiles during oblique impact, and to develop theoretical functions which can be used as a guide in the interpretation of ballistic data.

RESTRICTED
SECURITY INFORMATION

RESTRICTED

NPG REPORT NO. 954

Analytical Summary Part V Plastic flow in bars and shells

- (7) BALLISTIC SUMMARY. PART I. THE DEPENDENCE OF LIMIT VELOCITY ON PLATE THICKNESS AND OBLIQUITY AT LOW OBLIQUITY. NPG Report No. 2-46.

Object: To compare the results of ballistic test with the prediction of existing formulae, and with the results of theoretical analysis; to find the mathematical functions which best represent the fundamental relationship between limit velocity, plate thickness, and obliquity at low obliquity.

- (8) BALLISTIC SUMMARY. PART II. THE SCALE EFFECT AND THE OGIVE EFFECT. NPG Report No. 4-46

Object: To determine the effect of scale on ballistic performance, and to correlate the projectile nose shape with the results of ballistic test.

- (9) BALLISTIC SUMMARY. PART III. THE WINDSHIELD EFFECT, THE HOOD EFFECT, AND THE CAP EFFECT. (In preparation.)

Object: To determine the effect of windshields and hoods or caps on ballistic performance.

- (10) BALLISTIC SUMMARY. PART IV. THE DEPENDENCE OF LIMIT VELOCITY ON PLATE THICKNESS AND OBLIQUITY AT HIGH OBLIQUITY. (In preparation.)

Object: To compare the results of ballistic test with the results of theoretical analysis; to find mathematical functions which best represent the fundamental relationship between limit velocity, plate thickness, and obliquity at high obliquity.

- (11) BALLISTIC SUMMARY. PART V. THE CONSTRUCTION OF PLATE PENETRATION CHARTS OR TABLES. (In preparation.)

Object: To summarize the results of analysis in the form of standard charts or tables.

RESTRICTED
SECURITY INFORMATION

RESTRICTED

NPG REPORT NO. 954

Analytical Summary Part V Plastic flow in bars and shells

AUTHORITY

The material in this report is supplementary to the construction of plate penetration charts or tables. It was originally authorized by BUORD letter NP9/A9 (Re3) dated 9 January 1943, was later charged to Task Assignment NPG-41-Re3a-118-1, (Dynamics of Armor Penetration), and is currently charged to the foundational research program of the Naval Proving Ground.

OBJECT

To analyse the plastic flow in cylindrical bars and shells during impact against an unyielding plate.

RESTRICTED
SECURITY INFORMATION

Analytical Summary Part V Plastic flow in bars and shells

INTRODUCTION

A star crack is formed in a thin plate during impact by a pointed projectile. The petals at the impact are pushed back by the projectile during penetration and absorb energy. In order to obtain a guide in the calculation of this energy, especially for oblique impact, an analysis has been made of the plastic deformation of a plane triangular sheet or quadrant.

Part of the energy which is required by a projectile for the penetration of armor may be lost in the projectile itself. The energy may be stored in the plastic deformation of the projectile, or may be carried off in the form of kinetic energy by flying fragments. Even though the body of a service projectile is undeformed, the cap or hood and windshield usually absorb energy by deformation.

An analysis of the plastic deformation of a simple cylindrical shell under axial loading is given in the reports of references (1) to (4). An elementary theory of plastic deformation in cylindrical shells under other conditions of loading is given in the present report. A partial analysis of the plastic flow in a long cylindrical bar under impact loading has been published in the reports of references (13) to (20), and is summarized and reviewed in the present report. The published theory does not include the effects of irrotational flow, or of rotation of the principal axes of strain rate, which are therefore analysed in the present report.

The results of analysis are applied to the theory of armor penetration in references (24) and (25).

The state of strain has been defined throughout this series of reports in terms of the function

$$\frac{1}{3} \sqrt{(e_1 - e_2)^2 + (e_2 - e_3)^2 + (e_3 - e_1)^2}$$

in which e_1 , e_2 , e_3 are the principal components of the conventional strain, but this function has been incorrectly referred to as the octahedral shear strain. The true shearing displacement between octahedral

Analytical Summary Part V Plastic flow in bars and shells

planes is given by the expression

$$\sqrt{\frac{1}{3} \left\{ (1+e_1)^2 + (1+e_2)^2 + (1+e_3)^2 \right\} - \frac{3}{\frac{1}{(1+e_1)^2} + \frac{1}{(1+e_2)^2} + \frac{1}{(1+e_3)^2}}}$$

which may be simplified to the expression

$$\frac{2}{3} \sqrt{(e_1 - e_2)^2 + (e_2 - e_3)^2 + (e_3 - e_1)^2}$$

in the limiting case of small strains. This limiting expression, with the conventional strains e_1 , e_2 , e_3 replaced by the natural strains $\log(1+e_1)$, $\log(1+e_2)$, $\log(1+e_3)$, is frequently called the octahedral shear strain by contributors to the current literature.

The state of strain in an isotropic medium is actually defined by the three separate components of strain e_1 , e_2 , e_3 . The state of strain may be expressed in terms of any set of functions of these components. Thus it is convenient to use a set of cylindrical polar functions, of which the variable

$$\frac{1}{\sqrt{3}} \sqrt{(e_1 - e_2)^2 + (e_2 - e_3)^2 + (e_3 - e_1)^2}$$

is the radial coordinate. The use of any one of these three expressions is considered in these reports to be justified only on the basis of empirical representation, not on the basis of their accidental proportionality to the octahedral shear strain in the limiting case of small strains. The choice of factor between $\frac{1}{3}$, $\frac{2}{3}$, $\frac{1}{\sqrt{3}}$ is therefore arbitrary, but the term octahedral shear strain should properly be restricted to the factor $\frac{2}{3}$, if used at all, in conformity with the accepted convention. The function

$$\frac{1}{3} \sqrt{(e_1 - e_2)^2 + (e_2 - e_3)^2 + (e_3 - e_1)^2}$$

will therefore hereinafter be called the shear strain function.

Analytical Summary Part V Plastic flow in bars and shells

PLASTIC EQUILIBRIUM

The Plastic Deformation of a Triangular Sheet at Equilibrium.

Let an isocetes triangle be subject to symmetrical edge stresses on its base line and be free of stress on the two equal edges.

A complete analysis of the stress distribution in a triangle or sector would be complicated by the presence of both elastic and plastic zones. An analysis of the elastic deformation under a weak stress shows the point of initiation of plastic flow under increasing stress. A representative analysis has been completed for the special case of a quadrant.

The equations of elastic deformation have been reviewed in reference (22). The stress tensor Ψ is expressed in terms of the displacement Δr by the equation

$$\Psi = \lambda \nabla \cdot \Delta r I + \mu (\nabla \Delta r + \nabla^* \Delta r) \quad (1)$$

in which I is the unitary tensor, $\nabla \Delta r$ is the tensor gradient of Δr , $\nabla^* \Delta r$ is the transposed form of $\nabla \Delta r$, and λ , μ are elastic constants. The equation of equilibrium is

$$\nabla \cdot \Psi = (\lambda + \mu) \nabla \nabla \cdot \Delta r + \mu \nabla \cdot \nabla \Delta r = 0 \quad (2)$$

Let the components of displacement and stress be expressed in terms of cylindrical polar coordinates r , ϕ , z , and in terms of vectors of unit length ϵ_1 , ϵ_2 , ϵ_3 in the radial, azimuthal, and axial directions. The first particular solution of the equations of equilibrium is given by the equation

$$\Delta r = r^{\nu+1} \cos(\nu+2)\phi \epsilon_1 - r^{\nu+1} \sin(\nu+2)\phi \epsilon_2 \quad (3)$$

for which the components of stress are given by the equations

$$\begin{aligned} X_{11} &= +2\mu(\nu+1)r^\nu \cos(\nu+2)\phi \\ X_{22} &= -2\mu(\nu+1)r^\nu \cos(\nu+2)\phi \\ X_{12} &= -2\mu(\nu+1)r^\nu \sin(\nu+2)\phi \end{aligned} \quad (4)$$

The second particular solution of the equations of equilibrium is

Analytical Summary Part V Plastic flow in bars and shells

given by the equation

$$\begin{aligned} \Delta r = & + \left\{ (\nu+1 - \frac{5\lambda+6\mu}{3\lambda+2\mu}) r^{\nu+1} \cos \nu\phi - 2\nu(\nu+1) \frac{\lambda}{3\lambda+2\mu} z^2 r^{\nu-1} \cos \nu\phi \right\} \epsilon_1 \\ & - \left\{ (\nu+1 + \frac{5\lambda+6\mu}{3\lambda+2\mu}) r^{\nu+1} \sin \nu\phi - 2\nu(\nu+1) \frac{\lambda}{3\lambda+2\mu} z^2 r^{\nu-1} \sin \nu\phi \right\} \epsilon_2 \\ & + \left\{ 4(\nu+1) \frac{\lambda}{3\lambda+2\mu} z r^{\nu} \cos \nu\phi \right\} \epsilon_3 \end{aligned} \quad (5)$$

for which the components of stress are given by the equations

$$\begin{aligned} X_{11} = & + 2(\nu+1)(\nu-2)\mu r^{\nu} \cos \nu\phi - 4\nu(\nu^2-1) \frac{\lambda\mu}{3\lambda+2\mu} z^2 r^{\nu-2} \cos \nu\phi \\ X_{22} = & - 2(\nu+1)(\nu+2)\mu r^{\nu} \cos \nu\phi + 4\nu(\nu^2-1) \frac{\lambda\mu}{3\lambda+2\mu} z^2 r^{\nu-2} \cos \nu\phi \\ X_{12} = & - 2\nu(\nu+1)\mu r^{\nu} \sin \nu\phi + 4\nu(\nu^2-1) \frac{\lambda\mu}{3\lambda+2\mu} z^2 r^{\nu-2} \sin \nu\phi \end{aligned} \quad (6)$$

Both solutions are symmetric with respect to the median line at $\phi = 0$, and both solutions satisfy the boundary conditions at the plane faces of the sector, which are free of stress. A linear combination of the two solutions may be so adjusted as to satisfy the boundary conditions at the radial edges of the sector, which are also free of stress. The boundary conditions for a sector of arc $(1/N)2\pi$ are expressed by the equations

$$X_{12} = X_{22} = 0 \text{ at } \phi = \pm \frac{\pi}{N}, \quad z = 0 \quad (7)$$

The boundary equations are a pair of homogeneous linear equations in a pair of arbitrary constants, which can have a non trivial solution only if the determinant of the equations is zero. The determinant vanishes if the constant ν satisfies the transcendental equation

$$\sin 2(\nu+1) \frac{\pi}{N} + (\nu+1) \sin 2 \frac{\pi}{N} = 0 \quad (8)$$

The only real root of the equation is $\nu = -1$, which is the trivial value for a rigid displacement without strain. There is an infinite series of complex roots, however, the first few of which are listed in Table I for the case of a quadrant. The complex roots lead to complex functions for the displacement and stress. The real parts and the imaginary parts of the complex functions must separately satisfy the equations of equilibrium, and represent therefore a pair of independent solutions. A linear combination of pairs of solutions of all orders

Analytical Summary Part V Plastic flow in bars and shells

will give any arbitrary symmetric displacement at the arc of a sector or at the base of a triangle. The pair of lowest order is given in Table II for the case of a quadrant.

The functions in the table are so adjusted that the real and imaginary parts of X_{11} are equal to unity when $r = \sqrt{2}$ and $\phi = \pm \frac{\pi}{4}$. The functions are so arranged that the real parts are associated with the stretching and the imaginary parts are associated with the bending of a straight base line whose equation is $r \cos \phi = 1$. The normal stress across the base line varies from a compression stress at the center to a tension stress at the ends. The shear stress across the base line is zero at the center and is a maximum at the ends. The octahedral shear stress is a maximum at the ends of the base line.

As the base line is stretched and bent, a plastic zone appears and the shear stress on the base line is redistributed. Plastic flow occurs under the conditions of plane stress. The components of stress satisfy the condition of plastic yielding

$$\sqrt{X_{11}^2 - X_{11}X_{22} + X_{22}^2 + 3X_{12}^2} = X' \quad (9)$$

in which X' is the yield stress in the conventional tensile test. The yield condition is satisfied if the components of stress are expressed in terms of the parametric variables θ_1, θ_2 by the equations

$$\begin{aligned} X_{11} &= X' \sin \theta_1 - \frac{1}{\sqrt{3}} X' \cos \theta_1 \sin 2\theta_2 \\ X_{22} &= X' \sin \theta_1 + \frac{1}{\sqrt{3}} X' \cos \theta_1 \sin 2\theta_2 \\ X_{12} &= \frac{1}{\sqrt{3}} X' \cos \theta_1 \cos 2\theta_2 \end{aligned} \quad (10)$$

Let the components of stress be referred to cartesian axes and let θ_1, θ_2 be expressed in terms of cartesian coordinates x, y . The components of stress satisfy the equations of equilibrium

$$\begin{aligned} \frac{\partial X_{11}}{\partial x} + \frac{\partial X_{12}}{\partial y} &= 0 \\ \frac{\partial X_{12}}{\partial x} + \frac{\partial X_{22}}{\partial y} &= 0 \end{aligned} \quad (11)$$

Substitution of the functions of θ_1, θ_2 for the components of stress in

Analytical Summary Part V Plastic flow in bars and shells

the equations of equilibrium leads to a pair of homogeneous linear equations in the derivatives of θ_1 , θ_2 with respect to x , y . Linear combinations of the equations may be found which are exact differentials. The linear combinations are

$$\pm \frac{\sqrt{3}}{2} \frac{\sqrt{1 - \frac{4}{3} \sin^2 \theta_1}}{\cos \theta_1} \left(\frac{\partial \theta_1}{\partial x} dx + \frac{\partial \theta_1}{\partial y} dy \right) + \left(\frac{\partial \theta_2}{\partial x} dx + \frac{\partial \theta_2}{\partial y} dy \right) = 0 \quad (12)$$

if the differentials dx , dy satisfy the equation

$$\frac{dy}{dx} = \tan \left(\pm \frac{1}{2} \cos^{-1} \frac{1}{\sqrt{3}} \tan \theta_1 + \theta_2 - \frac{\pi}{4} \right) \quad (13)$$

This is the differential equation for the characteristics, along which the functions

$$\pm \frac{1}{2} \cos^{-1} \frac{(1 - \frac{4}{3} \sin^2 \theta_1)^{\frac{1}{2}}}{\cos \theta_1} + \theta_2$$

are constants. The change in θ_1 , θ_2 along a closed contour is zero. The change in θ_2 between any two characteristics of one family of characteristics is therefore constant along any characteristic of the other family of characteristics. The angle θ_2 is the angle between the plane of maximum shearing stress and the x axis. The angles between characteristics are bisected by the principal axes of stress.

Let the cartesian components of velocity in the plastic flow be \dot{x} , \dot{y} . The rate of strain is proportional to the deviation of the stress from isotropic tension, and the components of the rate of strain therefore satisfy the equations

$$\frac{\frac{\partial \dot{x}}{\partial x}}{2X_{11} - X_{22}} = \frac{\frac{1}{2} \left(\frac{\partial \dot{x}}{\partial y} + \frac{\partial \dot{y}}{\partial x} \right)}{3X_{12}} = \frac{\frac{\partial \dot{y}}{\partial y}}{2X_{22} - X_{11}} \geq 0 \quad (14)$$

Substitution of the functions of θ_1 , θ_2 for the components of stress in these equations leads to a pair of homogeneous linear equations in the derivatives of \dot{x} , \dot{y} with respect to x , y . Linear combinations of the equations may be found which are exact differentials along the characteristics.

Analytical Summary Part V Plastic flow in bars and shells

The linear combinations are

$$\left(\frac{\partial \dot{x}}{\partial x} dx + \frac{\partial \dot{x}}{\partial y} dy\right) + \frac{dy}{dx} \left(\frac{\partial \dot{y}}{\partial x} dx + \frac{\partial \dot{y}}{\partial y} dy\right) = 0 \quad (15)$$

The variation of the velocity vector along each characteristic is therefore everywhere orthogonal to the characteristic.

If the base of the triangle is stretched until the base line is completely plastic, then all active characteristics which pass through the base line terminate at the free edges of the triangle. The tangential velocity is zero along the inactive characteristics, which run into the elastic zone. Wherever inactive characteristics cross the base line, the directions of active characteristics are fixed by the boundary velocity. The angles θ_1 , θ_2 are constant along the free edges of the triangle. The characteristics are therefore straight in any region in which both families of characteristics are active, and the inactive characteristics are also straight. Characteristics for plastic flow, which are similar to the characteristics for elastic deformation, are illustrated by Figure (1).

The normal stress across the base line varies from a compression stress near the center to a tension stress near the ends. The shear stress across the base line is zero near the center, and is limited to $\frac{1}{2}X'$ near the ends where two principal components of stress are zero. The shear stress is greater than $\frac{1}{2}X'$ at intermediate points where there are two principal components of stress with opposite signs. The maximum possible shear stress is $\frac{1}{\sqrt{3}}X'$. The average shear stress is approximately $(.482)X'$.

The Plastic Deformation of a Cylindrical Shell at Equilibrium

That portion of any cylindrical shell on one side of a plane section through the shell applies to the portion on the other side a longitudinal component of force f_1 , along the axis of symmetry, a transverse component of force f_2 perpendicular to the axis of symmetry, and a bending moment M about a transverse axis. The components of force at equilibrium are constant along the axis of the shell, but the bending moment varies as a linear function of distance along the axis.

The stress tensor Ψ within the shell satisfies the vector equation

$$\bar{\nabla} \cdot \Psi = 0 \quad (16)$$

which may be expanded into a system of three scalar partial differential equations of the first order. Integration of these scalar equations by parts through the thickness of the shell gives the components of stress at

Analytical Summary Part V Plastic flow in bars and shells

the surfaces of the shell in terms of the components of stress in the interior.

It is assumed in the analysis that the shell is thin enough to permit the variation of stress through the thickness of the shell to be adequately represented by first order approximations. The integrals in the equations of equilibrium are then replaced by the stress resultants and by the stress moments in the shell. The major terms in the equations involve the stress resultants only. The major terms determine the components of force f_1 and f_2 , and the bending moment M . The minor terms in the equations involve both stress resultants and stress moments. The minor terms determine the distribution of stress near the point of application of a localized stress, and are only important around the point of application in a local zone which tends to contract with decrease in the thickness of the shell.

The components of stress at the surface of the shell satisfy the boundary conditions at the surface. The principal axes of stress at a free surface are parallel to the surface and the principal component of stress normal to the free surface is zero. The boundary conditions introduce terms into the equations of equilibrium which involve both the components of stress and the distortion of the shell. The boundary conditions determine the stability of the deformation.

The threshold for elastic instability under a longitudinal compression would be reached when the longitudinal force is nearly equal to

$$\frac{2\pi h^2 E}{\sqrt{3(1-\sigma^2)}}$$

in which E is Young's modulus, σ is Poisson's ratio, and h is the thickness of the shell. The critical force is the same for all shells of the same thickness regardless of their radii. The critical stress increases with decrease in radius, however, and a shell of small radius therefore yields first and then buckles.

The stress tensor Ψ in the shell under transverse stress has the components in the matrix

$$\begin{vmatrix} X_{11} & X_{12} & X_{s1} \\ X_{12} & X_{22} & X_{2s} \\ X_{s1} & X_{2s} & X_{ss} \end{vmatrix}$$

Analytical Summary Part V Plastic flow in bars and shells

Many of the components are small when the components are referred to the cylindrical polar coordinates r, ϕ, z . In the absence of stress from the free surfaces of the shell the components of stress nearly satisfy the relationships

$$X_{11} = X_{12} = X_{31} = 0 \quad (17)$$

The major terms in the equations of equilibrium are then

$$X_{22} = \frac{\partial X_{23}}{\partial z} = 0 \quad \frac{1}{r} \frac{\partial X_{23}}{\partial \phi} + \frac{\partial X_{33}}{\partial z} = 0 \quad (18)$$

The general solutions of these equations are

$$X_{23} = ru_1(\phi) \quad X_{33} = -zu_1'(\phi) + u_2(\phi) \quad (19)$$

in which $u_1(\phi)$ and $u_2(\phi)$ are arbitrary functions of ϕ . The functions $u_1(\phi)$ and $u_2(\phi)$ are determined by the boundary conditions at the ends of the cylindrical shell. A plane section through the shell remains a plane section if the functions $u_1(\phi)$ and $u_2(\phi)$ are harmonic functions of the form

$$u_1(\phi) = \alpha_0 + \alpha_1 \sin \phi \quad u_2(\phi) = \beta_0 + \beta_1 \cos \phi \quad (20)$$

in which the coefficient α_0 represents a uniform twist, the coefficient α_1 represents a transverse shear, the coefficient β_0 represents a uniform elongation, and the coefficient β_1 represents a uniform flexure. The resultant forces lie in the plane $\phi = 0$.

The components of stress cannot exceed the condition for plastic yielding

$$\sqrt{X_{33}^2 + 3X_{23}^2} = X' \quad (21)$$

in which X' is the yield stress in the conventional tension test.

In the special case of a cylindrical shell which is subject to a uniform longitudinal force, the function $u_1(\phi)$ is zero and the function $u_2(\phi)$ is constant. The shell yields when the component of force f_1 is given by the equation

$$f_1 = 2\pi ahX' \quad (22)$$

in which a is the radius of the shell and h is the thickness.

Analytical Summary Part V Plastic flow in bars and shells

In the special case of a cylindrical shell which is clamped at one end as a cantilever and is subject to a transverse force at the other end, the function $u_1(\phi)$ is variable, but the function $u_2(\phi)$ is zero.

If the length of the shell is greater than $a\sqrt{3}$, the plastic deformation of the shell is limited to two narrow zones next to the fixed end, where $\phi = 0$, and where $\phi = \pi$. The function $u_1(\phi)$ in the plastic range is given by the equations

$$u_1(\phi) = -\frac{X}{a\sqrt{3}} \sin \frac{a}{l} \sqrt{3}\phi \quad (-\phi' \leq \phi \leq +\phi') \quad (23)$$

$$u_1(\phi) = +\frac{X'}{a\sqrt{3}} \sin \frac{a}{l} \sqrt{3}(\phi - \pi) \quad (\pi - \phi' \leq \phi \leq \pi + \phi')$$

in which l is the length of the shell, and ϕ' is half the arc for each plastic zone. The function $u_1(\phi)$ in the elastic range of ϕ is given by the equations

$$u_1(\phi) = +\alpha_0 - \alpha_1 \sin \phi \quad (\phi' \leq \phi \leq \pi - \phi') \quad (24)$$

$$u_1(\phi) = -\alpha_0 + \alpha_1 \sin(\phi - \pi) \quad (\pi + \phi' \leq \phi \leq 2\pi - \phi')$$

in which the coefficients α_0 and α_1 are so chosen that $u_1(\phi)$ and $u_1'(\phi)$ are both continuous at the limit of the plastic range. The ultimate strength of the cantilever is reached when the component of force f_2 and the bending moment M at the fixed end satisfy the equations

$$lf_2 = M = \frac{4a^2 h X'}{1 - \frac{3a^2}{l^2}} \cos \frac{a}{l} \sqrt{3} \frac{\pi}{2} \quad (l \geq a\sqrt{3}) \quad (25)$$

If the length of the shell is less than $a\sqrt{3}$, the plastic zones are limited to regions where $\phi = \pm \frac{1}{2}\pi$. The plastic zones are parallel strips on each side of the shell, which extend the full length of the shell to the fixed end where they spread out into narrow zones next to the fixed end.

The function $u_1(\phi)$ in the elastic range of ϕ is given by the equation

$$u_1(\phi) = -\alpha_1 \sin \phi \quad \left(-\frac{1}{2}\pi + \phi' \leq \phi \leq +\frac{1}{2}\pi - \phi'\right) \quad (26)$$

Analytical Summary Part V Plastic flow in bars and shells

and the function $u_1(\phi)$ in the plastic range of ϕ is given by the equations

$$u_1(\phi) = -\frac{X'}{a\sqrt{3}} \sin \frac{a}{l\sqrt{3}} (\phi - \gamma) \quad \left(\frac{1}{2}\pi - \phi' \leq \pm \phi \leq \gamma + \frac{1}{\sqrt{3}} \frac{l}{a} \frac{\pi}{2}\right) \quad (27)$$

$$u_1(\phi) = -\frac{X'}{a\sqrt{3}} \quad \left(\gamma + \frac{1}{\sqrt{3}} \frac{l}{a} \frac{\pi}{2} \leq \pm \phi \leq \frac{1}{2}\pi\right)$$

The constants α_1 and γ are so chosen that $u_1(\phi)$ and $u_1'(\phi)$ are both continuous at the limits of the plastic range where $\phi = \pm \frac{1}{2}\pi \pm \phi'$. The ultimate strength of the shell is reached when the component of force f_2 and the bending moment M at the fixed end satisfy the equations

$$lf_2 = M = \frac{4alh \cdot X'}{l^2 \sqrt{3}} \cos \frac{1}{\sqrt{3}} \frac{l}{a} \frac{\pi}{2} \quad (l \leq a\sqrt{3}) \quad (28)$$

The plastic zones of uniform stress tend to spread out over the shell as the length of the shell is decreased.

In the limiting case of a short shell which is compressed between two plane frictionless surfaces, the plastic zone extends over nearly all of the shell. The resultant force f on each end of the shell is perpendicular to the frictionless surfaces. The components of force f_1 and f_2 are given in terms of the constant components of stress X_{23} and X_{33} in the plastic zone by the equations

$$f_1 = 2\pi ah X_{33} - 4ah X_{23} \tan \theta - f \cos \theta \quad (29)$$

$$f_2 = 4ah X_{23} = f \sin \theta \quad (30)$$

in which θ is the angle of obliquity between the normal to the plane surfaces and the axis of the shell. The force f itself is given in terms of the yield stress X' by the equation

$$f = \frac{2\pi ah X' \cos \theta}{\sqrt{1 + \frac{3}{4} \pi^2 \sin^2 \theta \cos^2 \theta}} \quad (31)$$

The Plastic Deformation of a Hood at Equilibrium

The hood of a common projectile is secured to the nose of the projectile with soft solder. The nose of the projectile applies to the hood a shear stress which is relatively small in comparison with the other stresses

Analytical Summary Part V Plastic flow in bars and shells

within the hood. The principal axes of stress at the nose of the projectile are therefore nearly parallel to the surface of the nose while the principal axes of stress at the free surface of the hood are truly parallel to the free surface. The condition of equilibrium for relative motion of the hood over the ogive is expressed by the equation

$$\frac{d}{dr}(rh'X_s) - h'(X_2 - rX_s) \sqrt{1 + \left(\frac{dz}{dr}\right)^2} = 0 \quad (32)$$

in which r , z are the cylindrical polar coordinates of a point on the nose contour, X_2 is the tangential stress in the circumferential direction, X_s is the tangential stress in the longitudinal direction, X_s is the yield stress of the solder in shear, and h' is the variable thickness of the hood. The components of stress under plastic flow satisfy the condition

$$\sqrt{X_2^2 - X_2X_s + X_s^2} = X' \quad (33)$$

in which X' is the stress in the conventional tensile test. The component of stress X_s is zero at the after edge of the hood and the components of stress at other positions may be found by integration of the equation of equilibrium. Near the tip of the hood where r is equal to zero, the equation of equilibrium for the hood becomes identical to the equation of equilibrium for an expanding hole in a thin plate.

The Static Deformation of Bars and Tubes of Mild Steel.

Several investigations of the elastic instability of thin walled cylinders under compression have been reported in the literature ^{1, 2, 3}. The longitudinal force which induces buckling depends upon the number of lobes which are formed. The actual force for two or more lobes has been found to be less than three fifths of the ideal force for a symmetrical wrinkle. The force is independent of radius when elastic buckling occurs, but the stress is constant when plastic yielding occurs. The force or stress is independent of the length of the cylinder.

Numerous static tests on bars and tubes under combined axial tension and internal pressure have been reported in the literature ^{10, 11, 12}. The strains in these tests are uniform as long as the forces in the specimen are increasing. When the rate of work hardening is balanced by the rate of contraction of diameter or thickness the forces in the specimen are at a maximum. The uniform strain then becomes unstable with respect to a localized strain and the specimen necks down or bulges

Analytical Summary Part V Plastic flow in bars and shells

out according to the type of loading. The specimen finally fractures in the neck or bulge. The fracture is circumferential under axial tension and is longitudinal under circumferential tension. Estimates of the stress and strain at fracture may be made on the basis of measurements of the decrease in thickness, the distortion of surface grids, and the curvatures of the specimen just prior to fracture.

The variation of strain in the neck of a round bar has been investigated by Bridgman⁶, who bored out tension test specimens and silver soldered cylindrical cores into the bores. When the composite specimens were pulled, each layer of silver solder outlined a deformation contour. At 92% reduction of area, the ratio a/R between the transverse radius a at the neck and the longitudinal radius R of the neck was 1.6, and the strain on the axis exceeded the average strain by 24%.

A plausible family of deformation contours have been derived from the photographs of sections through the specimens. A surface in the medium which was originally plane and orthogonal to the free surface before deformation, becomes curved* during deformation while it remains orthogonal to the free surface. If the curved surfaces in the neck were a family of confocal ellipsoids, the strain on the axis would exceed the average strain by 23%. The parametric equations for an ellipsoid in the neck are

$$z = \lambda \sqrt{a^2 + aR} \cos \theta \quad r = \sqrt{a^2 + aR} \sin \theta \quad (34)$$

in which r , z are cylindrical polar coordinates of a point on the ellipsoid and λ , θ are parameters, with $\lambda \ll 1$. The ellipsoid satisfies the limiting condition

$$\frac{dz}{dr} = -\frac{z}{R} \quad (r = a) \quad (35)$$

at the surface of the specimen. The ratio between the value of z on the

* The shape of the deformation contours might be revealed by a macroetch pattern in a suitably oriented specimen, but the patterns which have been examined so far have been inconclusive.

Analytical Summary Part V Plastic flow in bars and shells

axis and the average value of ε is given by the expression

$$\frac{\frac{3}{2} \frac{a}{R}}{1 + \frac{a}{R} - \frac{1}{\sqrt{1 + \frac{a}{R}}}}$$

from which the strains may be derived. The radii of curvature at the neck of a large number of specimens have been measured by Bridgman.

The variations of strain in the necks of rectangular bars have been investigated by Miklowitz⁹, who measured the distortion of grids on the surfaces and measured the variation in thickness. Representative strains in a square bar are illustrated by the table:

location	e_1	e_2	e_3
axis	(-.42)	(-.42)	(+1.93)
face	(-.34)	-.45	(+1.76)
edge	-.34	-.34	+1.30

in which e_1 , e_2 , e_3 are the strains perpendicular to a face, parallel to the face, and parallel to the axis. Measurements of surface strains do not determine the distribution of internal strain, and the internal strains, which are enclosed in parentheses, are plausible values, which are consistent with the measured average strain and the concave curvature of the faces.

The dimensions of the zone of necking in a strip of sheet steel are limited by restraints on the edges of the strip. The necking at the edge of the strip imposes a restraint on the distribution of strain in the center of the neck. A cross shaped depression is formed in the neck of a long strip with a decrease in thickness at the center which is twice the decrease in the thickness at the edge. The zone of necking is further limited by head restraint in a short strip, and the central depression is wide and short. The longitudinal radius of curvature R of the faces would be least in the limiting case of a strip with constrained edges. Thickness profiles in specimens with flanged edges have been measured by Baranski⁸. Specimens of various widths were compared in order to eliminate edge effects. The curvature of the neck increased slowly with elongation until the transverse restraints were established by necking in the flanges, but the final variation of curvature may be correlated with Bridgman's measurements of

Analytical Summary Part V Plastic flow in bars and shells

curvature if the variable

$$\frac{1}{\sqrt{2}} \frac{h}{R}$$

for a sheet of thickness h is assumed to be equivalent to the variable

$$\frac{a}{R}$$

for a bar of radius a .

The variation of stress in the neck of a round bar has been analysed by Bridgman⁷ who assumed that the flow stress is uniaxial with a constant magnitude but with a variable orientation, and assumed that the principal axis of tension is orthogonal to a family of paraboloids. An experimental check on Bridgman's correction is possible with the aid of published data on tubes and bars. An experimental determination of the correction was made by Korber and Muller⁵, who measured the contours of necked specimens at various stages of elongation, and then machined a series of new specimens to the measured contours. The machined specimens were first pulled to maximum load before machining, and were then pulled to fracture after machining. The experimental correction for necking is consistent with the calculated correction to within the experimental error. That the stress strain curves for tubes and round bars are the same for axial loading has been observed by Maier¹⁰ and by Davis and Parker¹². A value for the curvature in the neck of one particular tube has been given by Davis¹¹. The correction for necking in this tube is consistent with the correction for necking in a bar at the same strain.

The stress and strain in tubular specimens of mild steel have been measured by Maier and by Davis. The octahedral shear stress was nearly the same function of the shear strain function, for each combination of internal pressure and axial load. The specimens fractured when one principal component of stress reached a critical limit*, but the fracture stresses for longitudinal fractures were 25% less than the fracture stresses for circumferential fractures in the case of Davis' specimens, and was 12% less in the case of Maier's specimens. That the difference in stress is

* Davis quotes circumferential stresses which exceed the fracture stress for longitudinal fractures in specimens which fractured circumferentially, but the quoted values are not corrected for necking or bulging. Davis gives an estimate of the curvature of only one specimen. Inspection of the photographs of the specimens indicates that a correction for bulging in the other specimens would probably bring the stresses into agreement.

Analytical Summary Part V Plastic flow in bars and shells

probably the result of anisotropy between the axial and circumferential directions is shown by the data of Davis and Parker, who obtained a difference of only two or three percent. That there was no significant anisotropy between the radial and circumferential directions is probably shown by the similarity in the fractures of two of Davis' tubular specimens, which were cut from the original bar stock with the axes of the specimens parallel and perpendicular to the axis of the original bar stock. The specimens were tested under pure internal pressure, and fractured longitudinally with respect to their own axes. The data on tubular specimens are not inconsistent with the assumption that the fracture stress is increased by 4% for a 2-fold increase in shear strain function, and is independent of the isotropic tension as long as the isotropic tension is positive. The fracture stress in a tension test bar has, however, been shown by Bridgman⁶ to be increased by a prestrain under hydrostatic pressure, and the fracture stress in wire is increased by cold drawing. The fracture stress in a tubular specimen is less than the fracture stress in a tension test bar which is cut from the wall of the same tubular specimen. The fracture stress in a specimen may be influenced by size and shape. The fracture is propagated on a plane of maximum tension, or on a plane of maximum shear, or may switch from one plane to the other. The plane of propagation is influenced by the isotropic tension.

Data have been obtained at the Naval Proving Ground on the steel in the 37mm PP Type T21 projectiles. A longitudinal tension test specimen and a longitudinal compression test specimen were machined from one projectile and static stress-strain diagrams have been obtained.

The stress in the compression test was greater than the stress in the tension test at the same values of the shear strain function. The difference in stress was equivalent to an increase of 15% in the shear stress per 100,000 (lb)/(in)² increase in normal pressure.

Lead foil was used for lubrication in the compression test, but the lead foil was pinched off at the perimeter of the specimen, and the free surface was barrelled. The specimen was sectioned after compression and the section was polished and etched. Average deformation contours have been derived from the etch pattern and are illustrated by Figure (9). The deformation contours are not orthogonal to the interface between the specimen and the lead foil, as a result of a shear stress in the lead. The principal axes of stress at the interface were tilted three

Analytical Summary Part V Plastic flow in bars and shells

degrees out of the normal by the shear stress. The thickness of the specimen also varies with radius, and contributed to the variation in the orientation of the principal axes. A correction* which is valid in the limiting case of a thin specimen has been calculated and applied to the average stress in the specimen. The correction is based on the assumption that the shear stress at the interface is constant and is balanced by an isotropic pressure in the interior which is nearly uniform through the thickness of the specimen. The correction amounted to 15% at the final strain.

Metallographic examination of the compression specimen did not reveal any fractures in the specimen. Representative strains in the specimen are given in Table V. The static force-compression curve is given in Figure (3).

The upper and lower static yield points in the longitudinal tensile test were 33000 (lb)/(in)² and 30000 (lb)/(in)². The static tensile strength was 56000 (lb)/(in)². A cup and cone fracture occurred at 65% reduction of area. The stress in the neck has been corrected for curvature of the neck with the aid of Bridgman's data.

Miniature tension test specimens with circular test sections were cut from the bases of two other projectiles. The axes of tension in the specimens were transverse to the axes of the projectiles, and the test sections were offset four mm from the axes of the projectiles. The transverse ductility was less than the longitudinal ductility. A cylindrical ring was cut from the outermost layer of one projectile. The ring was carefully flattened out and was cut into tension test specimens with square test sections. The inner surface of the ring was located three mm from the free surface of the original projectile. The maximum strain at fracture in the ring, after flattening and pulling, was the same as the average strain at fracture in the miniature tensile specimens, and the tensile strength in the ring was greater than the tensile strength near the axis. The hardness of the projectile may not have been perfectly uniform.

The stress and strain at fracture in the specimens of the PP projectiles are summarized in Table VI. The principal components of stress X_1 , X_2 , X_3 , and the principal components of strain e_1 , e_2 , e_3 are the components in the radial, circumferential, and longitudinal axes of the projectile.

* The necessity for correction could be avoided by the use of platens and specimens with conical faces.

Analytical Summary Part V Plastic flow in bars and shells

The static stress-strain diagrams and the microstructure of the steel in the PP projectiles show that the projectiles are made of an annealed low carbon steel similar to the mild steel which has been extensively reported in the literature. The grain size was number 7 on the ASTM Scale of grain sizes. The thermal relaxation time for grains of this size is 2 microseconds.

PLASTIC FLOW

The Impact Compression of a Cylindrical Bar

The principal axes of stress at the free surface of the bar are always parallel to the free surface, and the principal component of stress normal to the free surface is zero. The principal axes of strain are also parallel to the surface of the bar, and a line element in the medium which was normal to the free surface before deformation is still normal after deformation.

A plane longitudinal compression wave is first generated in a long bar when it is struck on the end by a flat hammer. The longitudinal wave is propagated along the bar with a velocity equal to or greater than $(\kappa/\rho)^{1/2}$, in which κ is the bulk modulus of the medium and ρ is the density. The medium just behind the wave front is in a state of irrotational flow with a uniform particle velocity parallel to the axis of the bar. The strain in the longitudinal wave is uniaxial, with a finite component of strain in the direction of propagation, but with the other two components of strain equal to zero. The stress in the medium is a compression stress in the direction of propagation with a smaller compression stress in the plane of the wave front.

The initial longitudinal wave does not, therefore, satisfy the boundary conditions at the free surface of the bar, and is reflected and diffracted approximately as illustrated in Figure (5). Both longitudinal and transverse waves are required by the boundary conditions. The diffracted waves leave the free surface of the bar in a state of flow with a velocity which is greatest and perpendicular to the surface near the point of impact, but is least and at a small angle to the surface at a distance from the point of impact. The surface of the bar becomes distorted as the flow progresses. The distortion is controlled by a transverse wave of gradually increasing amplitude which transforms the radial motion into axial motion.

Analytical Summary Part V Plastic flow in bars and shells

In the limiting case of a slowly moving hammer the transverse wave is able to keep the particle velocity in the medium nearly uniform over a cross section of the bar. The motion of the bar is then given by von Karman's analysis^{15, 16, 19} of plastic waves. The equation of motion is

$$\rho \frac{\partial^2 \Delta z}{\partial t^2} = \frac{\partial}{\partial z} \left(\frac{X_s}{1+e_s} \right) = \frac{d}{de_s} \left(\frac{X_s}{1+e_s} \right) \frac{\partial^2 \Delta z}{\partial z^2} \quad (36)$$

in which Δz is the axial displacement of a particle in the medium, z is the initial coordinate of the particle, X_s is the stress along the axis of the bar, and e_s is the linear strain along the bar. The force on any section of a bar which was initially of unit cross sectional area is $X_s/(1+e_s)$. The strain e_s may be set equal to a function $\psi(z/t)$, and the displacement Δz is then given by the equation

$$\Delta z = - \int_x^\infty \psi \left(\frac{z}{t} \right) dz \quad (37)$$

The particle velocity $\dot{\Delta z}$ is given by the equation

$$\dot{\Delta z} = \int_x^\infty \frac{z}{t^2} \psi' \left(\frac{z}{t} \right) dz = - \int_0^{e_s} \left(\frac{z}{t} \right) de_s \quad (38)$$

Substitution of the function Δz into the equation of motion leads to the relationship

$$\frac{z}{t} = c = \sqrt{\frac{1}{\rho} \frac{d}{de_s} \left(\frac{X_s}{1+e_s} \right)} \quad (39)$$

in which c is the phase velocity. The particle velocity $\dot{\Delta z}$ is given in terms of the phase velocity c by the alternative equations

$$\dot{\Delta z} = - \int c de_s = - \frac{1}{\rho} \int \frac{1}{c} d \left(\frac{X_s}{1+e_s} \right) \quad (40)$$

The leading phase of the wave is elastic, and is propagated at the high velocity $(E/\rho)^{1/2}$. The elastic phase is trailed by a zone of increasing strain, and this zone is followed in turn by a plastic zone of uniform strain.

The leading phase of the primary wave in a bar with a free end is reflected from the end as an elastic unloading wave, which at first cancels the force in the bar. The unloading wave travels back along the bar until it encounters the plastic phase of the primary wave. The decrement in force which the unloading wave transmits is then reduced to a small fraction of its initial value as the unloading wave continues

Analytical Summary Part V Plastic flow in bars and shells

into the plastic zone, and a new elastic wave is propagated rapidly out again toward the free end of the bar. A new plastic zone begins at the boundary where the plastic phase of the primary wave has interacted with the elastic phase of the unloading wave. There is a difference of strain across this boundary after the interaction, but there can be no difference in the transmitted force or in the particle velocity. The ratio between the decrement of strain in the old plastic zone and the decrement of strain in the new plastic zone is therefore given qualitatively by the expression c^2/c_0^2 , in which c is the plastic phase velocity and c_0 is the elastic phase velocity. The ratio between the decrement of force in the old plastic zone and the increment of force in the new elastic wave is given qualitatively by the expression $2c/(c+c_0)$.

After the interaction between waves the unloading wave in the old plastic zone soon reaches the hammer, where it would be reflected without change in amplitude or phase if the hammer were rigid, and the new elastic wave soon reaches the free end of the bar where it is reflected as a new unloading wave.

The force in the plastic phase is decreased and the particle velocity is increased step by step as the elastic waves are reflected back and forth between the plastic zone and the free end of the bar. The plastic zone approaches the free end but never quite reaches it, because the frequency of reflection increases as the distance closes up. The progress of the plastic zone can be followed qualitatively by graphical methods¹⁷.

The force-compression curve has an inflection point at a particular value of the strain, and at this point the phase velocity c is a minimum. A larger strain than the critical strain for minimum phase velocity would be propagated at a greater velocity, and would overtake the critical strain. The formation of a shock wave is believed to occur when the impact velocity is greater than the particle velocity for a minimum phase velocity. The thickness of the shock wave in the direction of propagation is probably comparable with the radius of the bar. Associated with the shock wave is a radial displacement of the surface of the bar. The acceleration of the medium at the surface of the bar requires a dynamic pressure just ahead of the wave front and a dynamic tension just behind. The dynamic pressure sets the medium at the surface of the bar into motion in a radial direction, while the dynamic tension brings the radial motion to a stop. The dynamic pressure likewise displaces the medium along the axis of the bar in the direction of propagation, and the dynamic tension displaces the medium back again. The dynamic stress sets up a strain rate in the medium whose principal axis of compression has an outward direction from a central

Analytical Summary Part V Plastic flow in bars and shells

zone in the shock wave. Such a radial distribution of strain rate requires a plastic pressure for its maintenance. The force-compression curve for the shock wave is therefore higher than the force-compression curve for simple compression by the amount of dynamic stress and plastic pressure. The force-compression curve for the shock wave is a straight line which touches the force-compression curve for simple compression at two points, and is tangent to it at the lower point. The work done on unit volume of medium is equal to this area under the force-compression curve. The work done on unit volume in the shock wave is greater than the work done on unit volume in simple compression, even though the final strain is the same, because the principal axes of strain rate rotate with respect to the medium in the shock wave.

For each particle in the medium there is a value of z which represents the initial coordinate of the particle. Passing over the particle is some particular phase of the plastic wave. The phase velocity c is, by definition, the rate of increase in the value of z which is associated with the phase. The plastic wave therefore advances from particle to particle and moves away from the point of impact as long as c is finite*.

The shear strain function in the medium increases with increase in the impact velocity until the strain reaches that value for which there is a maximum in the adiabatic stress-strain curve for pure shear.

There would then be an instantaneous transition from homogeneous shear strain to localized shear strain, which is confined to a zone of infinitesimal thickness, if there were no heat conduction in the medium and if the flow stress were independent of strain rate. The localization of plastic flow is limited to a finite maximum rate and to zones of finite minimum thickness by the quenching effect of heat conduction.

* The actual velocity of propagation with respect to a stationary frame of reference is given by the equation

$$\frac{dz}{dt} + \frac{\partial \Delta z}{\partial z} \frac{dz}{dt} + \frac{\partial \Delta z}{\partial t} = c(1 + e_s) - f c d e_s$$

The actual velocity has a minimum at the inflection point in the force-compression curve. It has been postulated by White¹⁸ that a steady radial flow may develop near the point of impact if the impact velocity exceeds this minimum velocity of propagation. The energy per unit volume

Analytical Summary Part V Plastic flow in bars and shells

The transition may occur by one of two mechanisms.

In the first mechanism, a spontaneous transformation may occur, in which elastic energy in a specimen is converted into localized plastic energy. The dimensions of a steel specimen must be very large, however, for the occurrence of such a transformation.

In the second mechanism, deviations from thermal equilibrium are gradually amplified during a steady plastic flow. The deviations from thermal equilibrium arise from fluctuations in hardness from point to point in the medium.

During a static deformation, a specimen remains in thermal equilibrium, and the deformation may be continued beyond the maximum in the adiabatic stress strain curve without an appreciable localization of strain. A failure by shear may, however, still be initiated by a local failure by cleavage.

The fluctuations in temperature increase in amplitude with increase in strain rate. During a dynamic deformation, only the fine fluctuations in temperature are smoothed out by heat conduction, while the coarse fluctuations are nearly adiabatic, and the deformation may not be continued appreciably beyond the maximum in the curve without a severe localization of strain and a release of shear stress.

The velocity of propagation in a transverse wave vanishes when the deformation passes through the maximum in the adiabatic stress-strain curve for shear. In the limiting case of high velocity impact, there is a zone in the interior of the bar which is reached only by the longitudinal waves, and remains therefore essentially in a state of irrotational flow.

The velocity, in the case of cylindrical symmetry, may be expressed as a function of the cylindrical polar coordinates r , z and the time t .

of medium would then be a stationary function of position in the radial flow. The outermost boundary of the zone of radial flow would, however, increase in radius as the bar flowed into the zone of steady flow, and the circumferential strain at the outer boundary would steadily increase. In a ductile medium with a constant flow stress, the energy per unit volume would increase indefinitely with increase in strain, and the energy per unit volume of displaced medium within the zone of steady flow would therefore increase, whereas the flow of energy into the zone would be constant. It is evident, therefore, that a steady radial flow cannot be maintained in the absence of fracture or fusion of the medium.

Analytical Summary Part V Plastic flow in bars and shells

The coordinate r is the distance from the axis of the bar and the coordinate z is the distance from the plane face of the hammer. The velocity, in the case of irrotational incompressible flow, is the gradient of a scalar potential ψ which is a solution of Laplace's equation

$$\frac{1}{r} \frac{\partial}{\partial r} \left(r \frac{\partial \psi}{\partial r} \right) + \frac{\partial^2 \psi}{\partial z^2} = 0 \quad (41)$$

Let the velocity potential be referred to axes which move with the hammer. Before impact, the velocity potential ψ for unit impact velocity is z . Just after impact, the velocity potential is given by the series expansion

$$\psi = \sum c_m e^{-\lambda_m z} J_0(\lambda_m r) + z \quad (42)$$

in which $J_0(\lambda_m r)$ is a Bessel's function of zero order and c_m , λ_m are constants.

The derivatives of ψ are given by the equations

$$\begin{aligned} -\frac{\partial \psi}{\partial r} &= + \sum \lambda_m c_m e^{-\lambda_m z} J_1(\lambda_m r) \\ -\frac{\partial \psi}{\partial z} &= + \sum \lambda_m c_m e^{-\lambda_m z} J_0(\lambda_m r) - 1 \\ -\frac{\partial^2 \psi}{\partial r^2} &= + \sum \lambda_m^2 c_m e^{-\lambda_m z} \left\{ J_0(\lambda_m r) - \frac{1}{\lambda_m r} J_1(\lambda_m r) \right\} \\ -\frac{\partial^2 \psi}{\partial r \partial z} &= - \sum \lambda_m^2 c_m e^{-\lambda_m z} J_1(\lambda_m r) \\ -\frac{\partial^2 \psi}{\partial z^2} &= - \sum \lambda_m^2 c_m e^{-\lambda_m z} J_0(\lambda_m r) \end{aligned} \quad (43)$$

At the free surface of the bar, where the pressure is zero, the potential satisfies the boundary condition

$$\frac{\partial \psi}{\partial t} = \frac{1}{2} \{ (\nabla \phi)^2 - 1 \} \quad (44)$$

The rate of change of potential at a point which moves with the free

Analytical Summary Part V Plastic flow in bars and shells

surface is given by the equation

$$\frac{d\psi}{dt} = \frac{\partial\psi}{\partial t} - (\nabla\phi)^2 = -\frac{1}{2} \{(\nabla\phi)^2 + 1\} \quad (45)$$

The potential at the surface of a cylindrical bar which is just beginning to flow is still z , and the coefficients λ_m must satisfy the boundary conditions

$$J_0(\lambda_m a) = 0 \quad (r = a) \quad (46)$$

in which a is the radius of the bar. The axial component of the potential gradient would be zero at the surface of a rigid hammer. The coefficients c_m would then satisfy the condition

$$\sum \lambda_m c_m J_0(\lambda_m r) = +1 \quad (z = 0) \quad (47)$$

The functions $(\lambda_m r)^{\frac{1}{2}} J_0(\lambda_m r)$ are orthogonal in the interval $0 \leq r \leq a$ and the coefficients c_m may be evaluated by standard methods. They are given by equations of the form

$$\lambda_m c_m = \frac{2}{(\lambda_m a) J_1(\lambda_m a)} \quad (48)$$

Contours of equal velocity potential and stream-lines are given in Figure (6). The kinetic energy in the bar is given by the equation

$$\frac{1}{2\rho} \int (\nabla\psi)^2 d\tau = \frac{1}{2\rho} \int \psi \nabla\psi \cdot ds \quad (49)$$

in which τ is the volume of the bar and s is the surface area. The kinetic energy, when referred to stationary axes, is given by the equation

$$2\pi\rho a^3 \sum \frac{1}{(\lambda_m a)^3} = (.1618)\pi\rho a^3 \quad (50)$$

The series expansion gives a velocity at the free surface of the bar which is normal to the free surface. The radial velocity is small at a distance from the point of impact, but has a logarithmic singularity at the edge of the cylinder where $r = a$ and $z = 0$. In the neighborhood of the edge, the series expansion of the radial velocity is given by the limiting equation

$$-\frac{\partial\psi}{\partial r} = -.4244 - \frac{2}{\pi} \log z \quad (r = a, z \rightarrow 0) \quad (51)$$

Analytical Summary Part V Plastic flow in bars and shells

After a time interval the free surface of the bar is no longer cylindrical, and the potential at the free surface is no longer z . The potential in the bar may then be represented by the sum of two functions. The first function is just the series expansion, which satisfies the boundary conditions at the surface of impact, while the second function is dependent upon time, and satisfies the boundary conditions at the free surface. The second function may be generated by a continuous distribution of sources or sinks which are located just outside of the surface of a cylinder which extends from $z = -\infty$ to $z = +\infty$. The potential at the cylindrical surface is then given in terms of the density $q(z)$ of sources by the equation

$$\psi = \frac{a}{2\pi} \int_{-\infty}^{+\infty} \int_0^\pi \frac{q(\mu) d\mu d\phi}{\sqrt{(z - \mu)^2 + 4a^2 \sin^2 \frac{1}{2}\phi}} + z \quad (r = a) \quad (52)$$

and the derivatives of the potential are given by the equations

$$-\frac{\partial \psi}{\partial r} = -\frac{1}{2}q(z) + \frac{a^2}{2\pi} \int_{-\infty}^{+\infty} \int_0^\pi \frac{q(\mu)(1 - \cos\phi) d\mu d\phi}{\{(z - \mu)^2 + 4a^2 \sin^2 \frac{1}{2}\phi\}^{\frac{3}{2}}} \quad (r = a) \quad (53)$$

$$-\frac{\partial \psi}{\partial z} = +\frac{a}{2\pi} \int_{-\infty}^{+\infty} \int_0^\pi \frac{q(\mu)(z - \mu) d\mu d\phi}{\{(z - \mu)^2 + 4a^2 \sin^2 \frac{1}{2}\phi\}^{\frac{3}{2}}} - 1 \quad (r = a)$$

The substitutions

$$k = \frac{2a}{\sqrt{(z - \mu)^2 + 4a^2}} \quad \sin \frac{1}{2}\phi = \frac{\sqrt{1 - k^2 \sin^2 \theta}}{\sqrt{1 - k^2 \sin^2 \theta}} \quad (54)$$

introduce elliptic integrals. The potential at the cylindrical surface is then given by the equation

$$\psi = \frac{1}{2\pi} \int_{-\infty}^{+\infty} k F\left(\frac{\pi}{2}, k\right) q(\mu) d\mu + z \quad (r = a) \quad (55)$$

and the derivatives of the potential are given by the equations

$$-\frac{\partial \psi}{\partial r} = -\frac{1}{2}q(z) + \frac{1}{4\pi a} \int_{-\infty}^{+\infty} k \{F\left(\frac{\pi}{2}, k\right) - E\left(\frac{\pi}{2}, k\right)\} q(\mu) d\mu \quad (r = a) \quad (56)$$

$$-\frac{\partial \psi}{\partial z} = +\frac{1}{2\pi} \int_{-\infty}^{+\infty} \frac{k}{(z - \mu)} E\left(\frac{\pi}{2}, k\right) q(\mu) d\mu - 1 \quad (r = a)$$

Analytical Summary Part V Plastic flow in bars and shells

The boundary conditions at the surface of impact are undisturbed by the distribution of sources if the distribution is symmetric with respect to the plane $z = 0$.

The logarithmic singularity in the series expansion is cancelled for $z \geq 0$ if the source density $q(z)$ satisfies the limiting equation

$$q(z) = -\frac{4}{\pi} \log |z| \quad (z \rightarrow 0) \quad (57)$$

Inclusion of this logarithmic term in the source density introduces a surface potential whose derivative with respect to z is given at $z = 0$ by the limiting equation*

$$-\frac{\partial \psi}{\partial z} = -\frac{2}{\pi^2} \int_{-\infty}^{+\infty} \frac{k}{(z-\mu)^2} E\left(\frac{\pi}{2}, k\right) \log |\mu| d\mu - 1 = 0 \quad (r = a, z \rightarrow 0) \quad (58)$$

After a short time interval the surface of the bar is still nearly cylindrical, and the surface potential is still nearly equal to z . The partial derivatives of the potential at a cylinder of fixed radius a are still nearly equal to the partial derivatives at the free surface, and are given approximately by the series expansion. The potential is therefore given initially by a function ψ_1 which is a linear function of the time. The function ψ_1 satisfies the limiting equation

$$\psi = \frac{1}{2} t \left(\frac{\partial \psi}{\partial r} \right)^2 + z \quad (r = a) \quad (59)$$

in which the derivative with respect to r is given by the series expansion for zero time. As the flow continues, the potential deviates from the function ψ_1 . Insofar as the deviation is monotonic, the actual potential lies between the function ψ_1 and a function ψ_2 which satisfies the limiting equation

$$\psi = \frac{1}{2} t \left\{ \left(\frac{\partial \psi}{\partial r} \right)^2 + \left(\frac{\partial \psi}{\partial z} \right)^2 - 1 \right\} + z \quad (r = a) \quad (60)$$

* The limiting value of $kE\left(\frac{\pi}{2}, k\right)$ is $+1$ at $z = 0$. The integral may therefore be evaluated with the aid of the substitution of $(1+\alpha)z$ for μ , and with the aid of the relationship

$$\int_{-\infty}^{+\infty} \frac{1}{\mu - z} \log |\mu| d\mu = \int_0^1 \frac{1}{\alpha} \log \frac{1+\alpha}{1-\alpha} d\alpha + \int_1^{\infty} \frac{1}{\alpha} \log \frac{\alpha+1}{\alpha-1} d\alpha = 4\sum \frac{1}{(2m+1)^2} = \frac{1}{2}\pi^2$$

Analytical Summary Part V Plastic flow in bars and shells

The source density $q(z)$ has been so adjusted by trial that the potential is equal to ψ_2 with t set equal to $\frac{1}{3}$. The two limiting potentials for this time are compared in Table III. The potential ψ_1 has a minimum value of .2732 when z is .1556 a whereas the potential ψ_2 has a minimum value of .1387 when z is zero. The actual potential at $z = 0$ probably therefore satisfies the inequality

$$.1387 \leq \psi \leq .2732 \quad (r = a, z = 0)$$

The minimum in the potential ψ_1 varies with time and may be differentiated with respect to time.

A limit can then be estimated for the radial velocity, with the aid of the boundary condition

$$\frac{\partial \psi}{\partial t} = \frac{1}{2} \left(\left(\frac{\partial \psi}{\partial r} \right)^2 - 1 \right) \quad (r > a, z = 0) \quad (61)$$

and the estimated displacement of the moving edge of the bar is given by the integral

$$- \int \frac{\partial \psi}{\partial r} dt$$

The results of integration are given in Table IV. The estimated deformation contours after a time interval of one third are illustrated by Figure (7).

The series expansion gives a strain rate which decreases along the axis of the cylinder away from the point of impact, but increases along the radius at the surface of impact. The series expansion gives a maximum strain rate at the axis of the cylinder which approaches the limiting equation*

$$\frac{\partial^2 \psi}{\partial z^2} = (1.3262) \frac{1}{a} \quad (r = 0, z = 0) \quad (62)$$

* The strain rate on the axis of a cylinder of unit radius is given by the series expansion

$$\frac{\partial^2 \psi}{\partial z^2} = \sum \frac{2}{J_1(\lambda_m)} e^{-\lambda_m z} \quad (r = 0, a = 1)$$

which converges uniformly for $z > 0$ but diverges for $z \equiv 0$. The limit

Analytical Summary Part V Plastic flow in bars and shells

as z approaches zero, but gives a strain rate which is infinite at the edge of the cylinder where $r = a$ and $z = 0$.

If the irrotational flow were allowed to continue indefinitely, the flow in the bar would pass over into the steady flow in a stationary jet. The velocity potential in a cylindrical jet which impinges on a plane surface is identical to the velocity potential of two symmetrically opposing jets. The velocity potential is given by an application of Green's theorem,

$$4\pi\psi + \int \psi \nabla \left(\frac{1}{R} \right) \cdot ds - \int \frac{1}{R} \nabla \psi \cdot ds = 0 \quad (63)$$

in which R is the distance to a point on the free surface and s is the free surface with normal directed outward. At the free surface of the jets, the gradient of the stationary potential is constant in magnitude and parallel to the free surface. The potential is therefore given by the integral equation

$$\psi = \frac{1}{4} \pi \int \psi d\omega \quad (64)$$

in which ω is the solid angle of a circular section of the free surface. Formulae and tables which give the solid angle of a circular section are published in reference (23). The surface geometry of a jet has been adjusted by trial until the potential satisfies the integral equation. The calculations were aided by some observations on the geometry of a jet of tap water. Stream lines and contours of equal potential in the stationary jet are plotted in Figure (8).

which the series approaches as z approaches zero may be evaluated with the aid of a comparison between this series and the two auxiliary series

$$- \pi \sqrt{2} \sum_{n=1}^{\infty} (-1)^n \left(m - \frac{1}{4}\right)^{\frac{1}{2}} e^{-(m-\frac{1}{4})\pi z} \quad \text{and} \quad + \frac{\pi}{\sqrt{2}} \sum_{n=1}^{\infty} (-1)^n \int_{n-\frac{1}{4}}^{n+\frac{7}{4}} \mu^{\frac{1}{2}} e^{-\mu\pi z} d\mu$$

The differences between the three series are absolutely convergent, and their derivatives with respect to z are conditionally convergent at $z = 0$. The differences between the series may therefore be evaluated with z set equal to zero, while the limiting value of the third series as z approaches zero is just

$$- \frac{\pi}{\sqrt{2}} \int_{\frac{3}{4}}^{\frac{7}{4}} \mu^{\frac{1}{2}} d\mu = - 2.4666$$

Analytical Summary Part V Plastic flow in bars and shells

As the impact velocity approaches the velocity of sound in the medium, the zone of irrotational flow is compressed against the hammer. If the impact velocity were greater than the velocity of sound, a compression shock wave would probably be formed ahead of the hammer.

Plastic Flow in Cylindrical Projectiles

The British^{13, 14} have fired mild steel cylindrical projectiles against face hardened plate and have recorded the length of the undeformed part of each projectile. The dynamic yield point, for 0.2% compression, was estimated with the aid of an analysis of the propagation of elastic waves in the base of the projectile. The dynamic yield point was three times as large as the static yield point. The impact velocities were in the range from 380 (ft)/(sec) to 2750 (ft)/(sec), and the projectiles were mushroomed on impact.

The group at the California Institute of Technology¹⁹ have measured the distribution of strain in cylindrical bars after impact compression. The impact velocities were in the range from 22 (ft)/(sec) to 150 (ft)/(sec). The strain was uniform near the point of impact in all specimens of copper or steel. The tests included an annealed SAE 1020 steel with a yield point. When the impact velocity was 50 (ft)/(sec) or less the plastic strain at the point of impact was reported to be zero. It was therefore concluded that the elastic limit under dynamic loading was at least twice the yield point under static loading. The strain was uniform near the point of impact in specimens of lead when the impact velocity was small, but the specimens were mushroomed outward at the point of impact when the impact velocity was greater than 104 (ft)/(sec). Recently published²⁰ photographs* of the specimens show that the deformation is similar in appearance to the irrotational flow in Figure (7).

No dynamic stress-strain data on the steel in 37mm PP Type T21 projectiles are available, but the steel is probably similar to the mild steel which has been investigated by Manjoine and Nadai²¹. They obtained stress-strain diagrams on tensile specimens at various temperatures in the range from 20°C to 1200°C and at various strain rates from 10^{-6} (sec)⁻¹ to 10^9 (sec)⁻¹. At low temperatures the stress decreased and the ductility increased with increase in temperature. Strain aging occurred at high temperatures. The stress increased to a maximum and the ductility decreased to a minimum as the temperature was increased, through the strain aging range. When the temperature was increased still further, the stress again decreased with increase in temperature.

* These photographs were not previously available.

Analytical Summary Part V Plastic flow in bars and shells

At low temperatures the stress increased with increase in strain rate. At high temperatures, the strain aging range was shifted to a higher temperature by an increase in strain rate. The variation of stress with temperature and strain rate is illustrated by Figure (2).

The dynamic properties of the steel in the PP projectiles have been estimated, with the data for mild steel as a guide. At a strain rate of 1000 (sec)^{-1} the dynamic tensile strength is probably $84000 \text{ (lb)/(in)}^2$. An adiabatic force-strain curve for compression has been calculated and is plotted in Figure (3). This force-compression curve leads only to plastic shock waves. The phase velocity and the particle velocity in the shock waves are plotted in Figure (4).

The calculated maxima in the adiabatic stress strain curve for shear are summarized by Table IX. Two maxima occur in the adiabatic stress-strain curve as the result of strain-aging. The formation of a fault, if it starts at all, probably does not continue indefinitely with the formation of an open fracture, but is trapped instead by strain-aging.

The beveled faces of five 37mm PP Type T21 projectiles have been machined off flat to form cylinders with sharp edges. The length of each projectile was 3.90 (in) and the mass of each projectile was 1.84 (lb) after machining. The five projectiles were fired with velocities in the range from 650 (ft)/(sec) to 1450 (ft)/(sec) against 3" Class A Plate No. 55E652B5, which was polished slightly by the impacts. The projectiles would not hold a permanent magnetization, and the impact velocities could not be obtained with the conventional magnetic solenoids. The velocity of one projectile was measured with contact screens. The velocities of the other projectiles were estimated on the basis of the weight of powder charge.

The projectiles were sectioned and etched after impact. Profiles of the projectiles are illustrated in Figure (11). Deformation contours have been derived from the etch pattern of one projectile and are plotted in Figure (10). Representative strains in the projectile are listed in Table VII. The principal components e_1 , e_2 , e_3 of strain are the components in the radial, circumferential, and longitudinal directions of the original projectile. The strains at the edge are estimated on the assumption that the final strain may be represented by a combination of compression in the longitudinal axis and a fold at the edge. The principal axes of strain would remain orthogonal to the surfaces during such a deformation. The strain was a pure compression on the axis of the projectile, but varied from shear at the impact surface to tension at the free surface near the edge of the projectile.

Analytical Summary Part V Plastic flow in bars and shells

Several projectiles fractured on impact. The fractures were propagated along two different surfaces of maximum shear stress. The occurrence of two surfaces of fracture may be correlated with the anisotropy of the steel and with the calculations of strain near the edge. At the impact surface, where the strain was a shear, the fracture surface contains the radial axis, even though this is the more ductile of the three surfaces of maximum shear stress. At the free surface, where the strain was a symmetrical tension, the fracture surface contains the longitudinal axis, and is the less ductile of the two surfaces of equal shear stress.

The projectiles fractured into petals which remained attached to the projectiles. The edge of the circular face of each projectile became the tips of the petals. The circumferential strain at fracture may be estimated with the aid of measurements of the total width of the tips of the petals. It is assumed that no appreciable circumferential deformation occurred in the petals after the release of stress by fracture. The circumferential strains are listed in Table VIII. The projectiles fractured when the shear strain function was equal to .30

The first maximum in the adiabatic stress-strain curve for shear occurs at a shear strain function equal to $.50 \pm .05$. A homogeneous adiabatic tension becomes unstable with respect to a localized adiabatic shear at a shear strain function equal to .9. It is therefore unlikely that the observed fractures arose from an adiabatic instability. The shear fractures were probably initiated by cleavage fractures. The difference between the shear strain functions for an adiabatic cleavage and a static cleavage is a result of the difference in flow stress. After an adiabatic strain in tension to a shear strain function equal to .30, the temperature is 70°C , and the dynamic flow stress at the edge of the projectile is $125000(\text{lb})/(\text{in})^2$, whereas fracture in the static tests occurred at a shear strain function of .74 and at a tension stress of $126000(\text{lb})/(\text{in})^2$. The agreement between these calculated values of the fracture stress is gratifying, but may be fortuitous.

Analytical Summary Part V Plastic flow in bars and shells

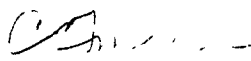
The computations for this report were performed by:
V. L. Nichols and J. M. Foster
Mathematical Physics Branch,
Computation and Ballistics Department

The analyses and interpretations in this report were conducted by:
A. V. Hershey, Head of Mathematical Physics Branch,
Computation and Ballistics Department

The report was prepared by:
A. V. Hershey, Head of Mathematical Physics Branch,
Computation and Ballistics Department

This report was reviewed by:
F. W. Dresch, Director of Computation and Ballistics,
Computation and Ballistics Department
C. C. Bramble, Director of Research, Ordnance Group

APPROVED J. F. BYRNE
Captain, USN
Commander, Naval Proving Ground


C. T. MAURO
Captain, USN
Ordnance Officer
By direction

UNANNOUNCED

UNCLASSIFIED

U. S. Naval Proving Ground
Dahlgren, Virginia

14

NPG ~~SECRET~~ -954

2

LIBRARY OF CONGRESS
REFERENCE DEPARTMENT
TECHNICAL INFORMATION DIVISION
FORMERLY
(NAVY RESEARCH SECTION)

~~SECRET~~
~~SECRET~~
~~SECRET~~

JUL 22 1952

(21) ~~Final~~ Partial Report, No. 3
on
The Foundational Research Program
of the
Naval Proving Ground

9

Final Report

6

Analytical Summary, Part V.
Plastic Flow in Bars and Shells.

DOD/DC
REFERENCE
AUG 9 1972
REGULATED
76 A

(10) A. V. / Heisterkamp

(11) 14 July 52

Copy No.:
No. of Pages: 38

(12) 10-pp /

Date:

JUL 14 1952

DECLASSIFIED
DOD DIR 5200.9

~~SECRET~~
~~SECRET~~
~~SECRET~~

UNCLASSIFIED

251 575 ✓

mk

UNCLASSIFIED

NPG REPORT NO. 954

Analytical Summary Part V Plastic flow in bars and shells

TABLE I

Complex roots of the transcendental equation

$$\sin 2(v+1)\frac{\pi}{4} + (v+1)\sin\frac{2\pi}{4} = 0$$

order	v
1	1.740 ± 1.119 i
2	5.845 ± 1.681 i
3	9.885 ± 1.970 i
4	13.908 ± 2.167 i

UNCLASSIFIED

SECURITY INFORMATION

Analytical Summary Part V Plastic flow in bars and shells

TABLE II

First order solution of elastic equations for a steel quadrant

 $2\mu\Delta r$

$r^{2.740} \sin(1.119 \log r)$	$r^{2.740} \cos(1.119 \log r)$	
-.0253 +.1169 i	-.0586 -.0631 i	$\sin(1.740\varphi) \sinh(1.119\varphi)$
+.0586 +.0631 i	-.0253 +.1169 i	$\cos(1.740\varphi) \cosh(1.119\varphi)$
-.0743 -.2568 i	+.1173 -.1328 i	$\sin(3.740\varphi) \sinh(1.119\varphi)$
-.1173 +.1328 i	-.0743 -.2568 i	$\cos(3.740\varphi) \cosh(1.119\varphi)$

 $2\mu r\Delta\varphi$

$r^{2.740} \sin(1.119 \log r)$	$r^{2.740} \cos(1.119 \log r)$	
-.0854 -.4832 i	+.2256 -.1362 i	$\sin(1.740\varphi) \cosh(1.119\varphi)$
-.2256 +.1362 i	-.0854 -.4832 i	$\cos(1.740\varphi) \sinh(1.119\varphi)$
+.1173 -.1328 i	+.0743 +.2568 i	$\sin(3.740\varphi) \cosh(1.119\varphi)$
-.0743 -.2568 i	+.1173 -.1328 i	$\cos(3.740\varphi) \sinh(1.119\varphi)$

 X_{11}

$r^{1.740} \sin(1.119 \log r)$	$r^{1.740} \cos(1.119 \log r)$	
+.113 +.273 i	-.122 +.213 i	$\sin(1.740\varphi) \sinh(1.119\varphi)$
+.122 -.213 i	+.113 +.273 i	$\cos(1.740\varphi) \cosh(1.119\varphi)$
-.335 -.555 i	+.238 -.651 i	$\sin(3.740\varphi) \sinh(1.119\varphi)$
-.238 +.651 i	-.335 -.555 i	$\cos(3.740\varphi) \cosh(1.119\varphi)$

Analytical Summary Part V Plastic flow in bars and shells

TABLE II (continued)

 X_{22}

$r^{1.740} \sin(1.119 \log r)$	$r^{1.740} \cos(1.119 \log r)$	
+ .388 - .779 i	+ .410 + .880 i	$\sin(1.740\varphi) \sinh(1.119\varphi)$
- .410 - .880 i	+ .388 - .779 i	$\cos(1.740\varphi) \cosh(1.119\varphi)$
+ .335 + .555 i	- .238 + .651 i	$\sin(3.740\varphi) \sinh(1.119\varphi)$
+ .238 - .651 i	+ .335 + .555 i	$\cos(3.740\varphi) \cosh(1.119\varphi)$

 X_{12}

$r^{1.740} \sin(1.119 \log r)$	$r^{1.740} \cos(1.119 \log r)$	
- .266 - .334 i	+ .138 - .526 i	$\sin(1.740\varphi) \cosh(1.119\varphi)$
- .138 + .526 i	- .266 - .334 i	$\cos(1.740\varphi) \sinh(1.119\varphi)$
+ .238 - .651 i	+ .335 + .555 i	$\sin(3.740\varphi) \cosh(1.119\varphi)$
- .335 - .555 i	+ .238 - .651 i	$\cos(3.740\varphi) \sinh(1.119\varphi)$

RESTRICTED

NPG REPORT NO. 954

Analytical Summary Part V Plastic flow in bars and shells

TABLE III

A comparison between the limiting potentials, for a cylinder of unit radius, at a time equal to one third

$\frac{z}{a}$	0	.1	.2	.4	.6	.8	1.0
ψ_1	∞	.2990	.2825	.4224	.6074	.8027	1.0010
ψ_2	.1387	.1704	.2377	.4114	.6038	.8014	1.0005

RESTRICTED
SECURITY INFORMATION

Analytical Summary Part V Plastic flow in bars and shells

TABLE IV

The estimated radial displacement of the edge of a cylindrical bar of unit radius, during irrotational flow after impact at unit velocity

t	.0001	.0010	0100	.1000	.3333
$-\frac{\partial\psi}{\partial r}$	4.84	3.61	2.48	1.61	1.31
$-\int\frac{\partial\psi}{\partial r}dt$.0005	.0041	.030	.197	.53

Analytical Summary Part V Plastic flow in bars and shells

TABLE V

The final strain on the median plane of a compression specimen of the steel in the 37mm PP Type T21 projectile. The specimen was initially a cylinder, .492" diam. x .5" gage length.

location	center	edge
e_1	+ 1.32	+ .18
e_2	+ 1.32	+ 1.30
e_3	- .81	- .63
$\frac{1}{3} \sqrt{\sum (e_m - e_n)^2}$	1.01	.79

Analytical Summary Part V Plastic flow in bars and shells

TABLE VI

The approximate stress and strain at fracture of the steel in 37mm PP Type T21 projectiles at a tensile strength of 56000 (lb)/(in)²

specimen	longitudinal	transverse	transverse
cross section	.505" diam.	.126" diam.	.125" square
gage length	1"	.5"	.5"
% reduction of area	64.7	58.1	52.9
fracture	cup and cone	cup and cone*	shear*
X_1	+ 31000	+ 23000	+ 21000
X_2	+ 31000	+ 121000	+ 126000
X_3	+ 133000	+ 23000	+ 21000
$\frac{1}{3} \Sigma X_n$	+ 65000	+ 56000	+ 56000
e_1	- .44	- .39	- .33
e_2	- .44	+ 1.64	+ 1.23
e_3	+ 2.19	- .39	- .33
$\frac{1}{3} \sqrt{\Sigma (e_n - e_n)^2}$	1.24	.96	.74

*The structure of the fracture was broken up by a relatively coarse transverse fiber.

Analytical Summary Part V Plastic flow in bars and shells

TABLE VII

Approximate strains in a 37mm PP Type T21 projectile after impact at 654 (ft)/(sec).

location	center, impact face	edge, impact face	edge, free surface
e_1	+ .60	+ .04	- .18
e_2	+ .60	+ .47	+ .47
e_3	- .61	- .34	- .17
$\frac{1}{\sqrt{2}} \sqrt{\sum (e_m - e_n)^2}$.57	.33	.30

Analytical Summary Part V Plastic flow in bars and shells

TABLE VIII

Impact tests with .37mm PP Type T21 projectiles. Initial diameter of projectiles was 3.69 cm.

Impact Velocity (ft)/(sec)	Upset Diameter cm	Fracture	e_2	$\frac{1}{3} \sqrt{\sum (e_n - e_n)^2}$
(650)	5.31	none	.44	.29
654	5.42	none	.47	.30
(650)	5.58	incipient	.51	.33
(650)	5.84	incipient	.57	.36
(1000)	8.1	shear	.46	.30
(1450)	12.5	shear	.48	.31

SECRET

RESTRICTED

NPG REPORT NO. 954

Analytical Summary Part V Plastic flow in bars and shells

TABLE IX

The estimated shear strain function at the maxima and minimum in the adiabatic stress strain curve for shear in the steel of the 37mm PP Type T21 projectiles at a strain rate of 1000 (sec)⁻¹.

	max	min	max
$\frac{1}{3} \sqrt{\sum (e_m - e_n)^2}$.5	1.3	3.0

RESTRICTED
SECURITY INFORMATION

Analytical Summary Part V Plastic flow in bars and shells

APPENDIX B - LIST OF SYMBOLS

a	radius of a cylindrical shell or cylindrical bar
α	variable of integration
$\alpha_0, \alpha_1, \beta_0, \beta_1$	arbitrary constants in the functions for cylindrical shells
c	plastic phase velocity
c_0	elastic phase velocity
c_n	coefficients in the series expansion of velocity potential
λ	arbitrary constant in the functions for cylindrical shells
e_1, e_2, e_3	principal components of strain
E	Young's modulus
$\epsilon_1, \epsilon_2, \epsilon_3$	unit vectors in the radial, azimuthal, and axial directions
$E(\frac{\pi}{2}, k)$	elliptic integral of amplitude $\frac{1}{2}\pi$ and modulus k
f	force
f_1	longitudinal component of force
f_2	transverse component of force
$F(\frac{\pi}{2}, k)$	elliptic integral of amplitude $\frac{1}{2}\pi$ and modulus k
ϕ'	half the arc of a plastic zone in a cylindrical shell
h	uniform thickness of a shell

Analytical Summary Part V Plastic flow in bars and shells

h'	variable thickness of a shell
i	$\sqrt{-1}$
I	identity tensor
$J_0(\lambda_m r), J_1(\lambda_m r)$	Bessel's functions
κ	bulk modulus
l	length of a cylindrical shell
λ_m	constants in the series expansion of velocity potential
λ, μ	elastic moduli
λ, θ	parametric variables for deformation contours in the neck of a cylindrical bar
M	bending moment
μ	variable of integration
N	symmetry number of a sector
ν	complex index in the elastic equations for a plane sector
ω	solid angle
ψ	velocity potential
ψ_1	initial velocity potential
ψ_2	limiting velocity potential
$\psi(\frac{z}{t}), \psi'(\frac{z}{t})$	strain distribution and its derivative for a von Karman wave
Ψ	stress tensor
$q(z)$	source density for irrotational flow in a bar

Analytical Summary Part V Plastic flow in bars and shells

r, ϕ, z	cylindrical polar coordinates
r	position vector
Δr	displacement
R	spherical polar coordinate
R	radius of curvature
ρ	density
s	surface
σ	Poisson's ratio
t	time
τ	volume
θ	angle of obliquity
θ_1, θ_2	parametric coordinates of characteristics for plane plastic stress
$u_1(\phi), u_2(\phi)$	arbitrary functions in the equilibrium of a cylindrical shell
v	particle velocity
x, y, z	Cartesian coordinates
$\dot{x}, \dot{y}, \dot{z}$	components of velocity
X'	yield stress in tension (steel)
X_s	yield stress in shear (solder)
X_1, X_2, X_3	principal components of stress
$X_{11}, X_{22}, X_{33},$ X_{23}, X_{31}, X_{12}	polar components of stress

RESTRICTED
SECURITY INFORMATION

Analytical Summary Part V Plastic flow in bars and shells

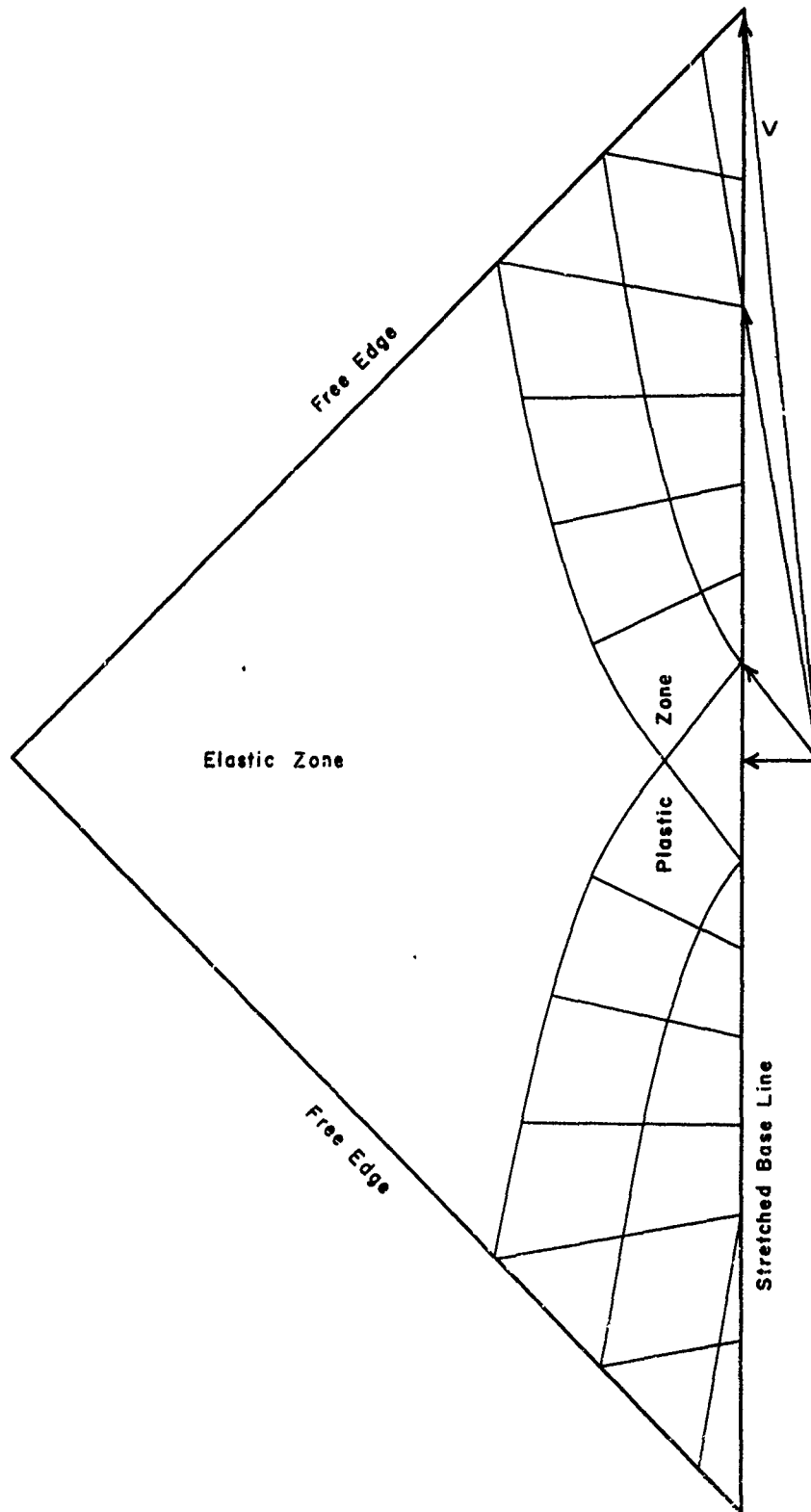
BIBLIOGRAPHY

- (1) "The Strength of Thin Cylindrical Shells as Columns," W. M. Wilson and N. M. Newmark, Univ. Illinois Eng. Expr. Sta., Bull. No. 255. (Feb 1933).
- (2) "Strength Tests of Thin-Walled Duralumin Cylinders in Compression," E. E. Lundquist, NACA Report No. 473 (1933).
- (3) "Methods and Formulas for Calculating the Strength of Plate and Shell Constructions as Used in Airplane Design," O. S. Heck and H. Ebner, NACA Tech. Memo. No. 785 (Feb 1936).
- (4) "Formulas for Stress and Strain," R. J. Roark, (Mc Graw Hill, New York, 1938) p. 272.
- (5) "Die Verfestigung metallischer Werkstoffe beim Zug und Druckversuch," F. Korber and H. Muller, Mitt. Kaiser Wilhelm Inst. Eisenforschung, Düsseldorf 8, 181 (1926).
- (6) "On The Effect of Prestraining in Tension on the Behavior of Steel in Tension," P. W. Bridgman, WAL Report No. 111/7-6 (June 1944).
- (7) "The Stress Distribution at the Neck of a Tension Specimen," P. W. Bridgman, Trans. ASM 32, 553 (1944).
- (8) "Zerreissversuche bei ebener plastischer Verformung," G. Baranski, Z. Metallkunde 26, 173 (1934).
- (9) "The Influence of the Dimensional Factors on the Mode of Yielding and Fracture in Medium Carbon Steel. I. The Geometry and Size of the Flat Tensile Bar," J. Miklowitz, J. App. Mech. 15, 274 (1948).
- (10) "Einfluss des Spannungszustandes auf das Formanderungsvermogen der metallischen Werkstoffe," A. F. Maier, (V.D I. Verlag Berlin, 1935).
- (11) "Yielding and Fracture of Medium Carbon Steel Under Combined Stress," E. A. Davis, J. App. Mech. 12, A-12 (Mar 1945).
- (12) "Behavior of Steel Under Biaxial Stress as Determined by Tests on Tubes," H. E. Davis and E. R. Parker, J. App. Mech. 15, 201 (1948).
- (13) "The Compressive Strength of Mild Steel Cylindrical Projectiles at Varying Striking Velocities," British Report R. C. 186 (Jan 1941).

Analytical Summary Part V Plastic flow in bars and shells

- (14) "The Use of Flat-Ended Projectiles for Determining Dynamic Yield Stress. I. Theoretical Considerations," G. I. Taylor, Proc. Roy. Soc. A194, 289 (1948); "II. Tests on Various Metallic Materials," A. C. Whiffin, Proc. Roy. Soc. A194, 300 (1948).
- (15) "Wave Propagation In a Uniform Bar Whose Stress-Strain Curve is Concave Upward," M. P. White and Le V. Griffis, NDRC Report No. A-152 (Feb 1943).
- (16) "The Force Produced by Impact of a Cylindrical Body," M. P. White, NDRC Report No. A-157 (Mar 1943). "The Propagation of Plasticity in Uniaxial Compression," M. P. White and Le V. Griffis, J. App. Mech. 15, 256 (1948).
- (17) "The behavior of Longitudinal Stress Waves Near Discontinuities in Bars of Plastic Material," Le V. Griffis, NDRC Report No. A-212 (Sept 1943).
- (18) "On The Impact Behavior of a Material with a Yield Point," M. P. White, J. App. Mech. 16, 39 (1949).
- (19) "Behavior of Metals Under Dynamic Conditions. The Propagation of Plastic Strain in Compression," P. E. Duwez, D. S. Clark and H. E. Martens, NDRC Report No. M-302 (July 1944).
- (20) "The Propagation of Plasticity in Uniaxial Compression," D. S. Clark, J. App. Mech. 16, 219 (1949).
- (21) "Influence of Rate of Strain and Temperature on Yield Stresses of Mild Steel," M. Manjoine, J. App. Mech. 11, A-211 (Dec 1944).
- (22) Analytical Summary Part I. The physical Properties of STS Under Triaxial Stress. NPG Report No. 6-46.
- (23) Analytical Summary Part III. Plastic Flow in Armor Plate. NPG Report No. 864.
- (24) Analytical Summary Part VI. The Theory of Projectile Ricochet. (In preperation).
- (25) Ballistic Summary Part III. The Windshield Effect, the Hood Effect, and the Cap Effect. (In preperation).

FIGURE (1)

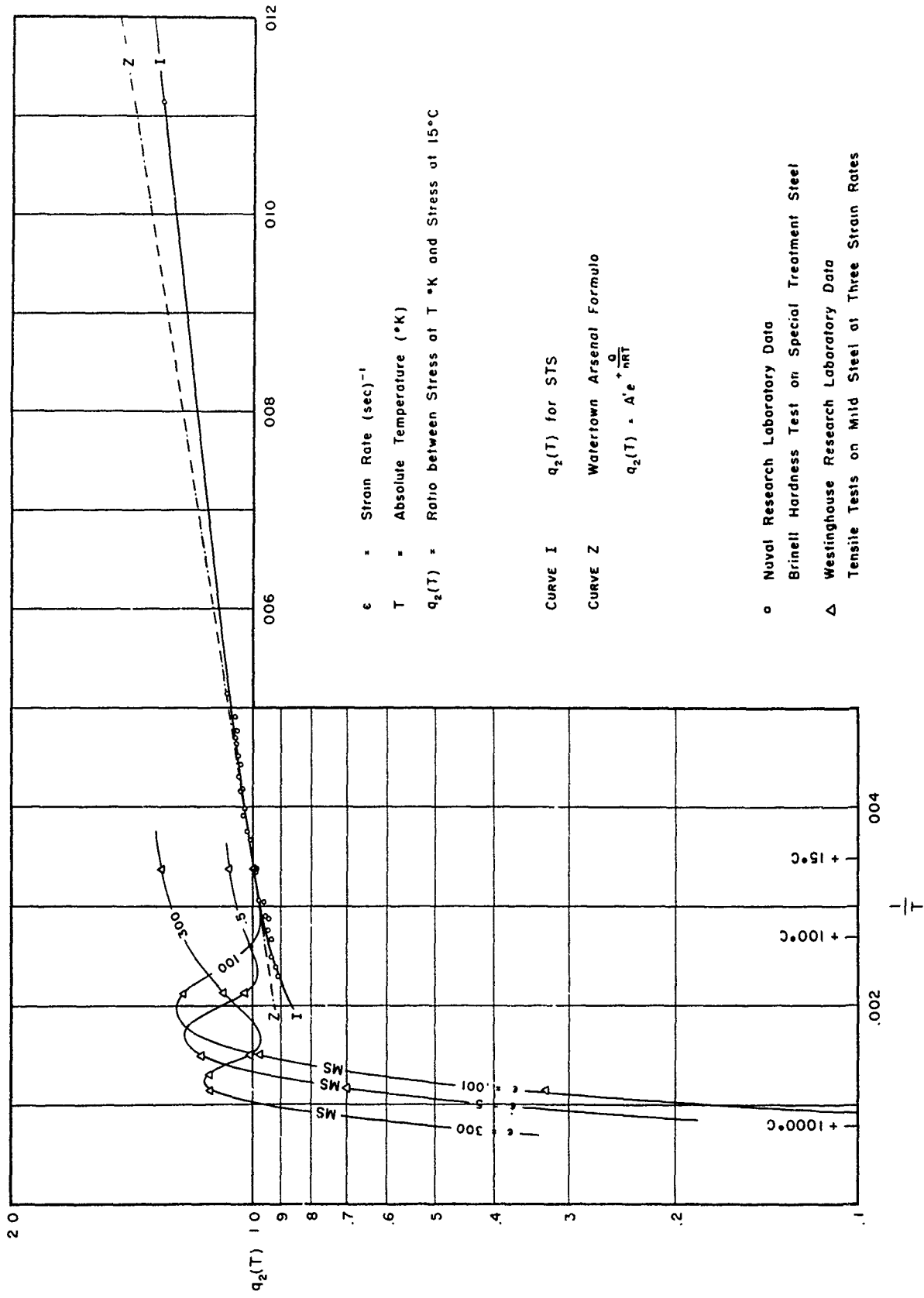


CHARACTERISTICS FOR PLASTIC FLOW IN AN ISOCELES TRIANGLE

NPG PHOTO NO 3095 (APL)

THE VARIATION OF STRESS WITH TEMPERATURE

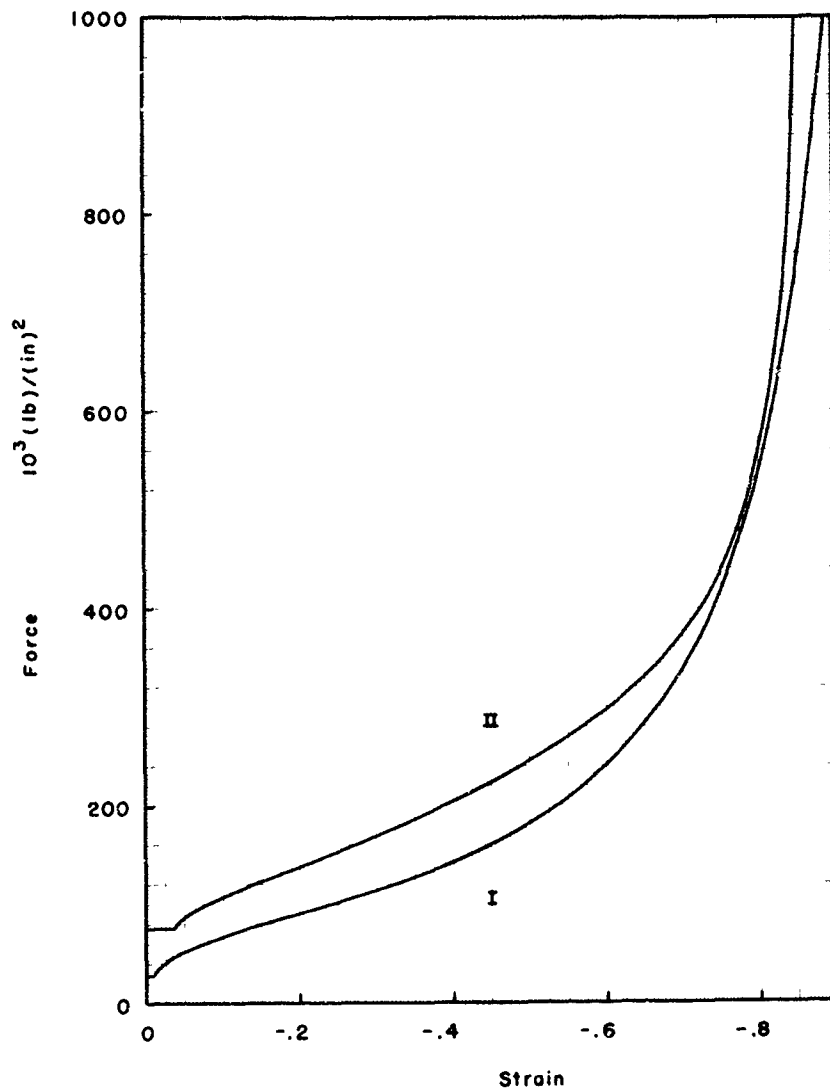
FIGURE 2



NP9-48530

FIGURE (3)

FORCE-COMPRESSION CURVES FOR BARS OF PP PROJECTILE STEEL

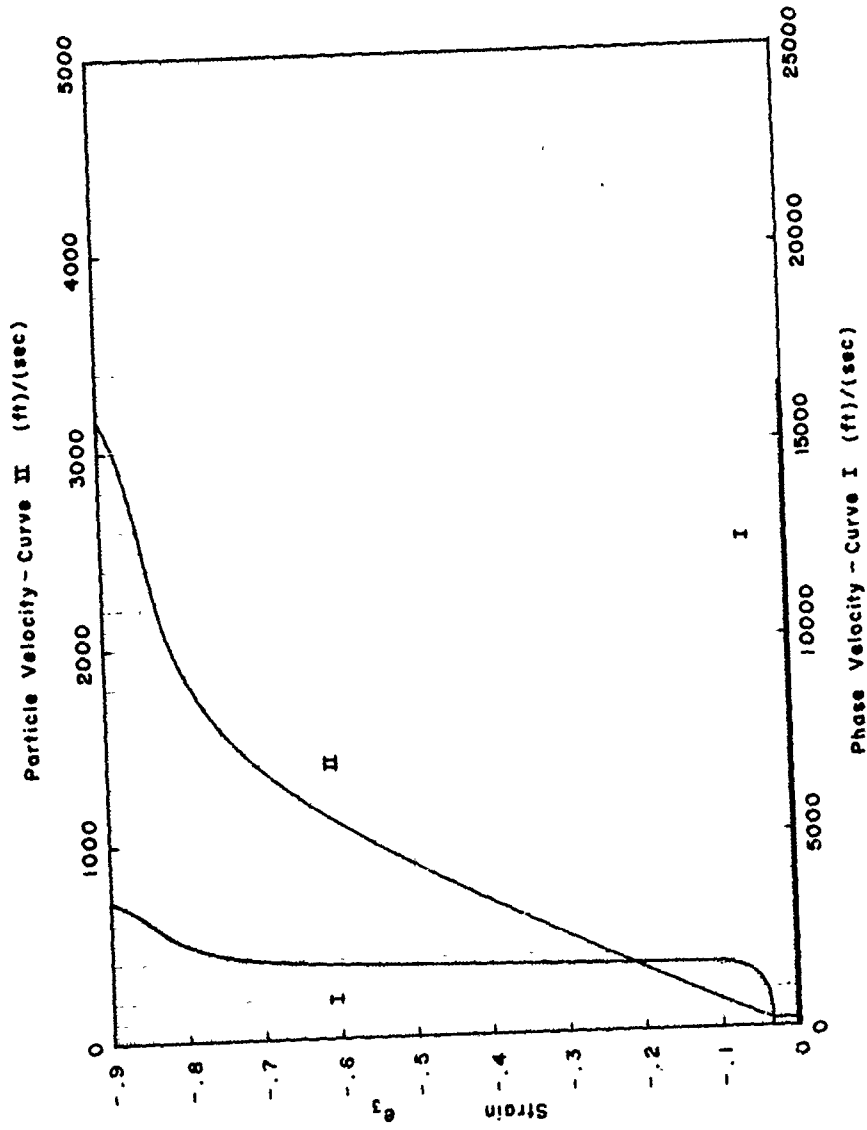


Curve I Static Isothermal Compression

Curve II Dynamic Adiabatic Compression

NP9-48531

FIGURE (4)

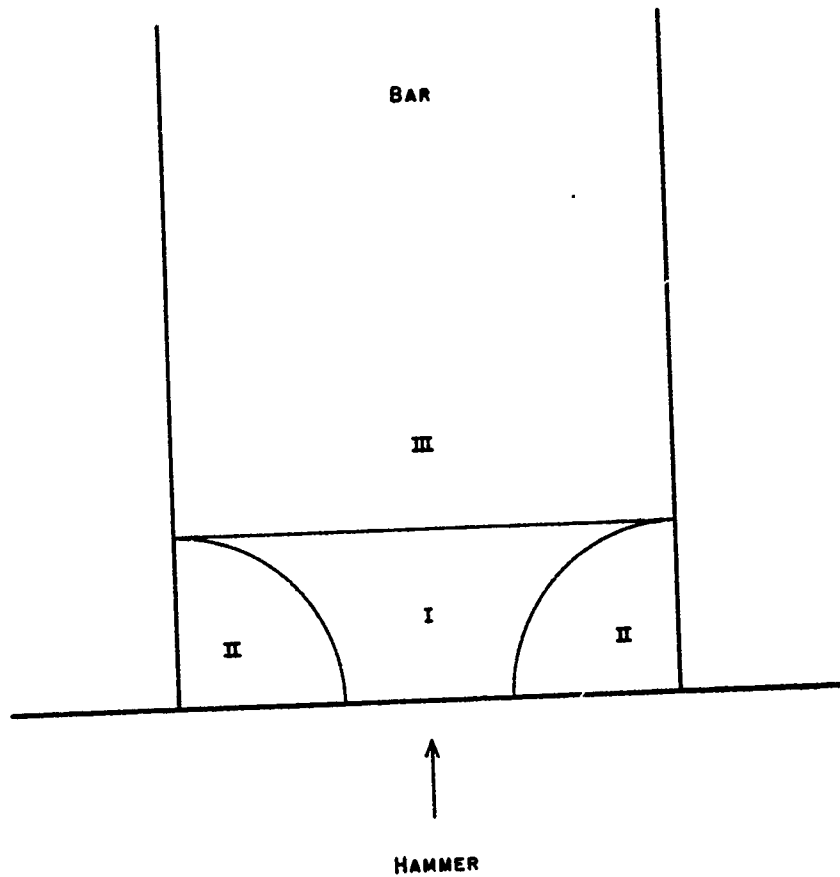


THE PROPAGATION OF COMPRESSION WAVES IN BARS OF PP PROJECTILE STEEL

NP9-48532

FIGURE (5)

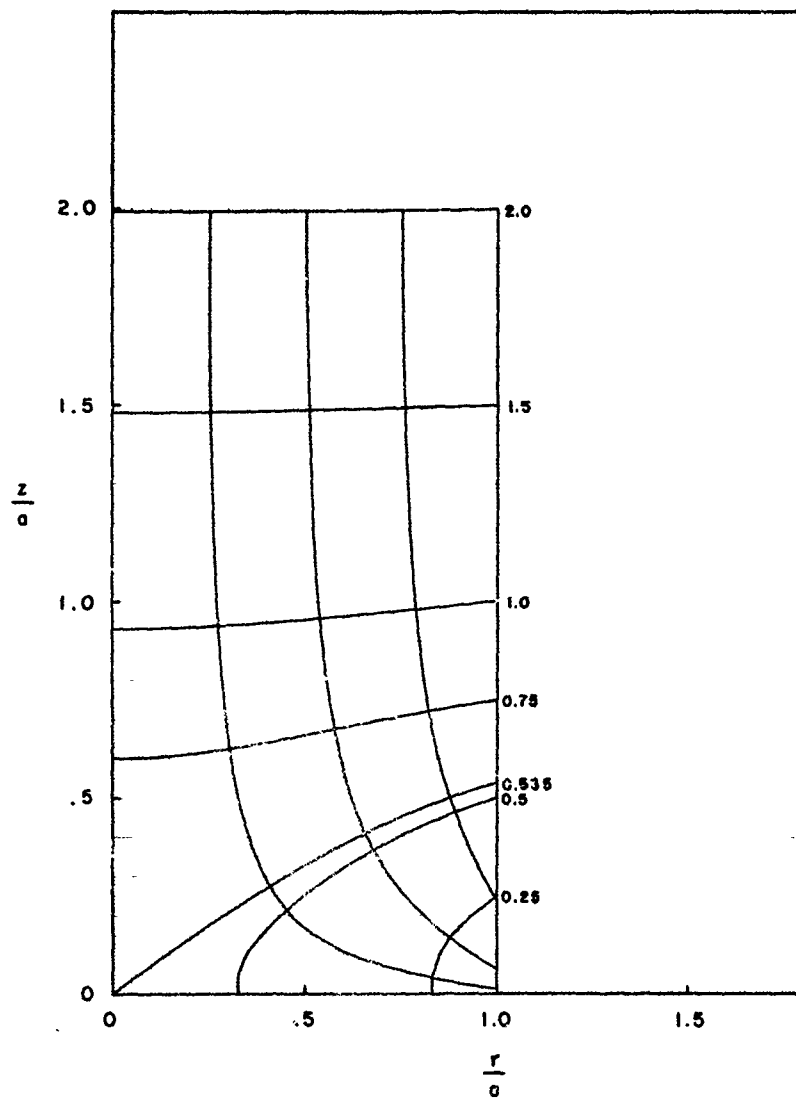
THE COMPRESSION WAVE IN A CYLINDRICAL BAR ON IMPACT



- ZONE I Constant High Pressure
- ZONE II Variable Intermediate Pressure
- ZONE III Undeviated Zero Pressure

NP9-48533

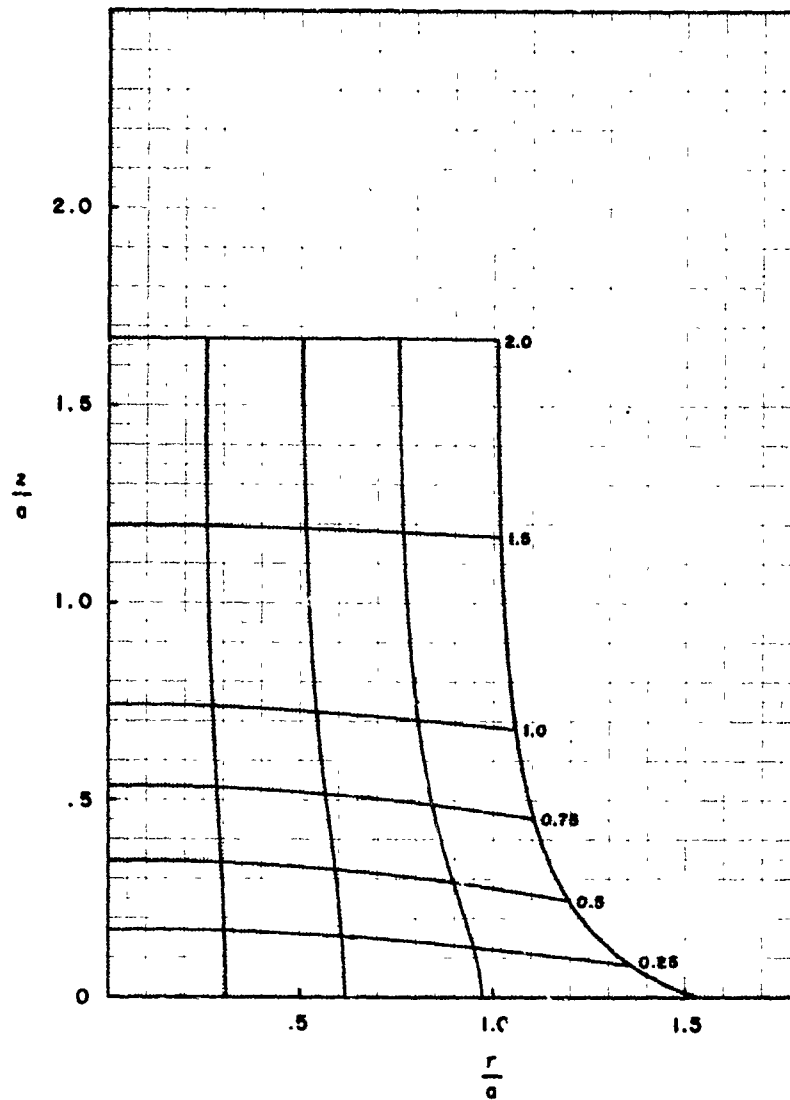
FIGURE (6)



CONTOURS OF EQUAL VELOCITY POTENTIAL AND STREAM-LINES
FOR IRROTATIONAL FLOW IN A CYLINDRICAL BAR

NP9-48534

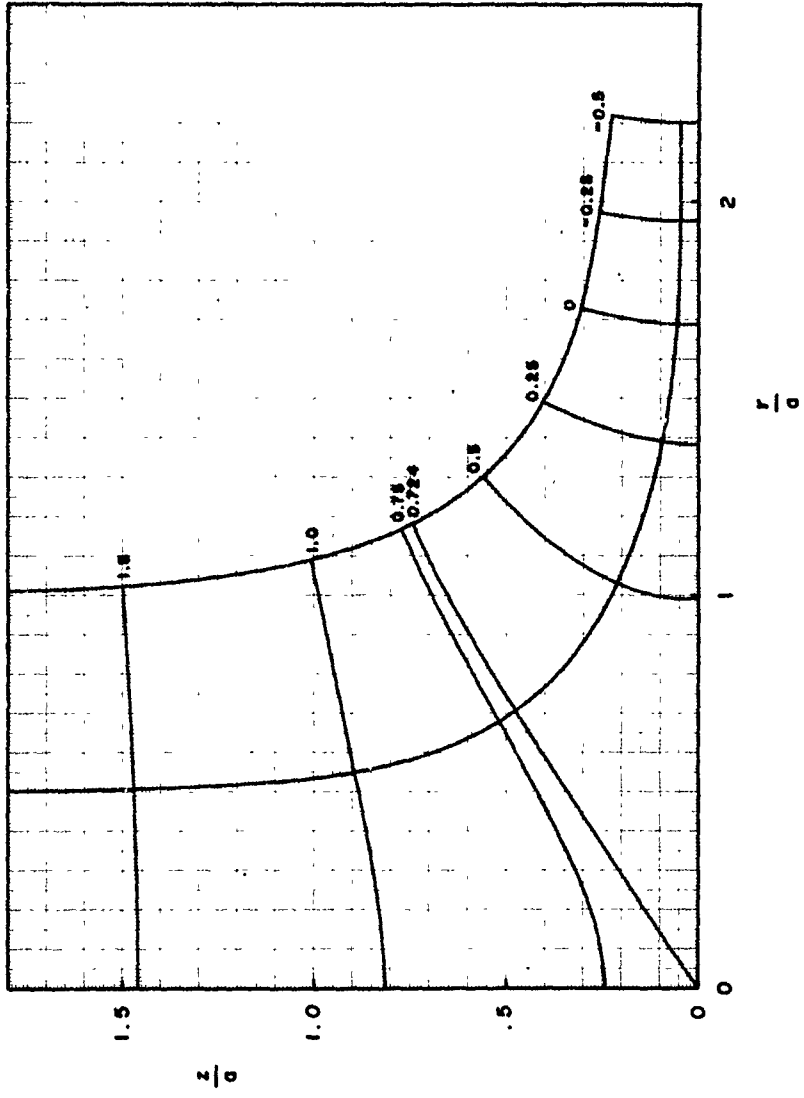
FIGURE (7)



DEFORMATION CONTOURS FOR IRROTATIONAL FLOW
IN A CYLINDRICAL BAR UNDER IMPACT

NP9-48535

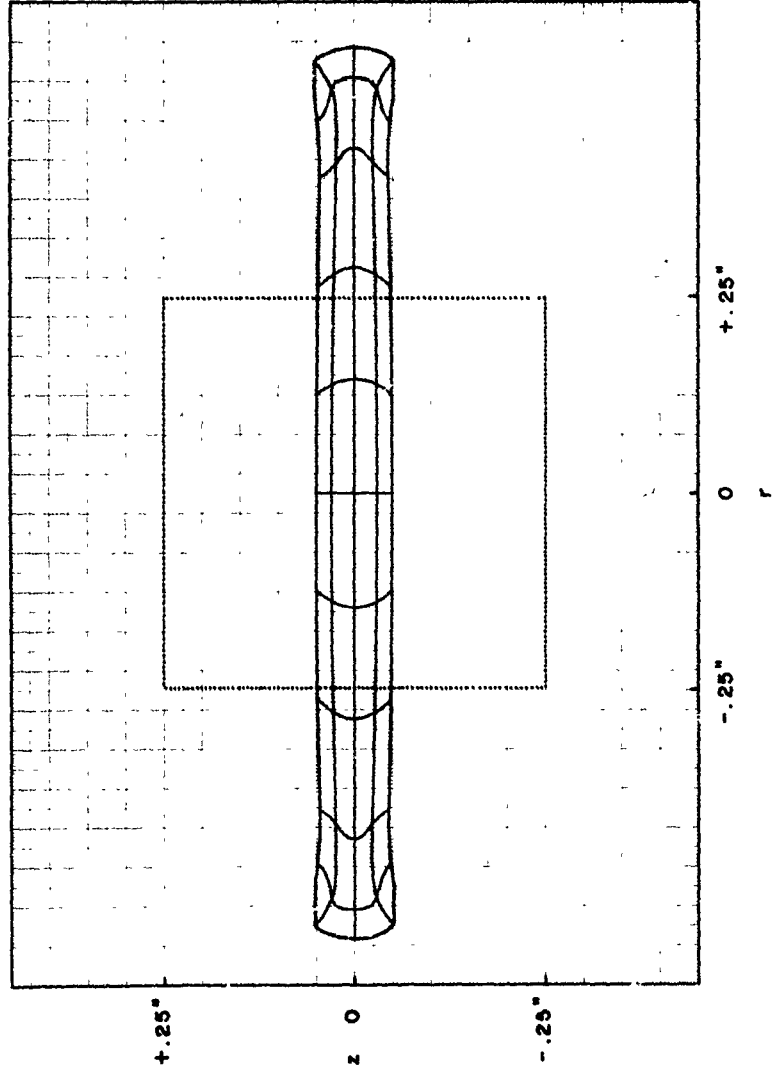
FIGURE (8)



CONTOURS OF EQUAL VELOCITY POTENTIAL AND STREAM-LINES
FOR IRROTATIONAL FLOW IN A STEADY JET

NPS-48536

FIGURE (9)



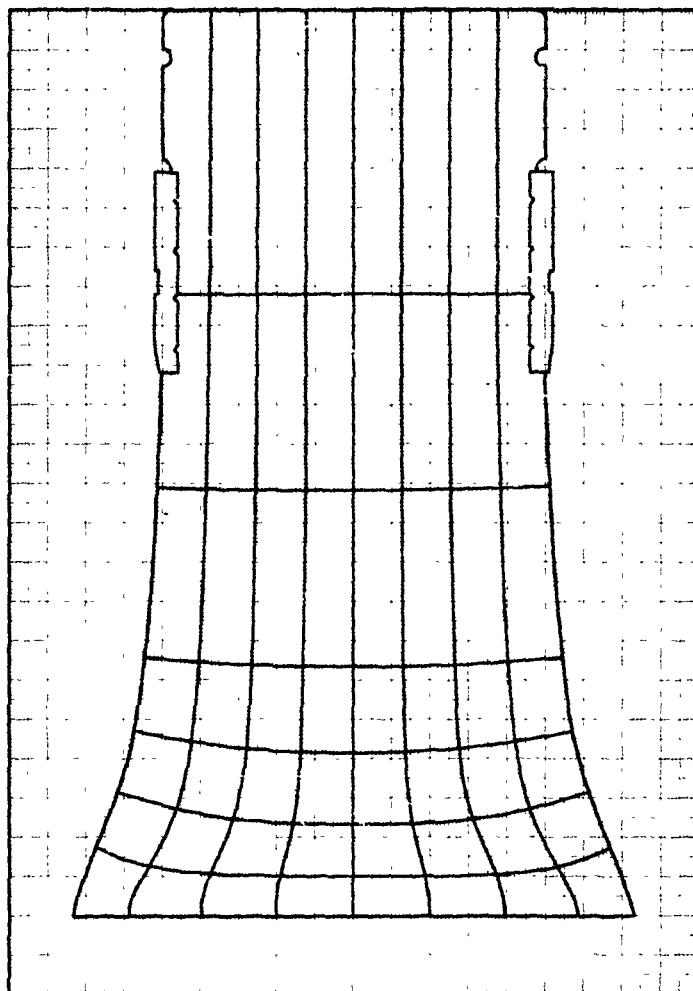
DEFORMATION CONTOURS FOR THE COMPRESSION TEST

37 mm PP Type T21 Projectile

Specimen = .5" x .5" diam. Cylinder

NP9-48537

FIGURE (10)

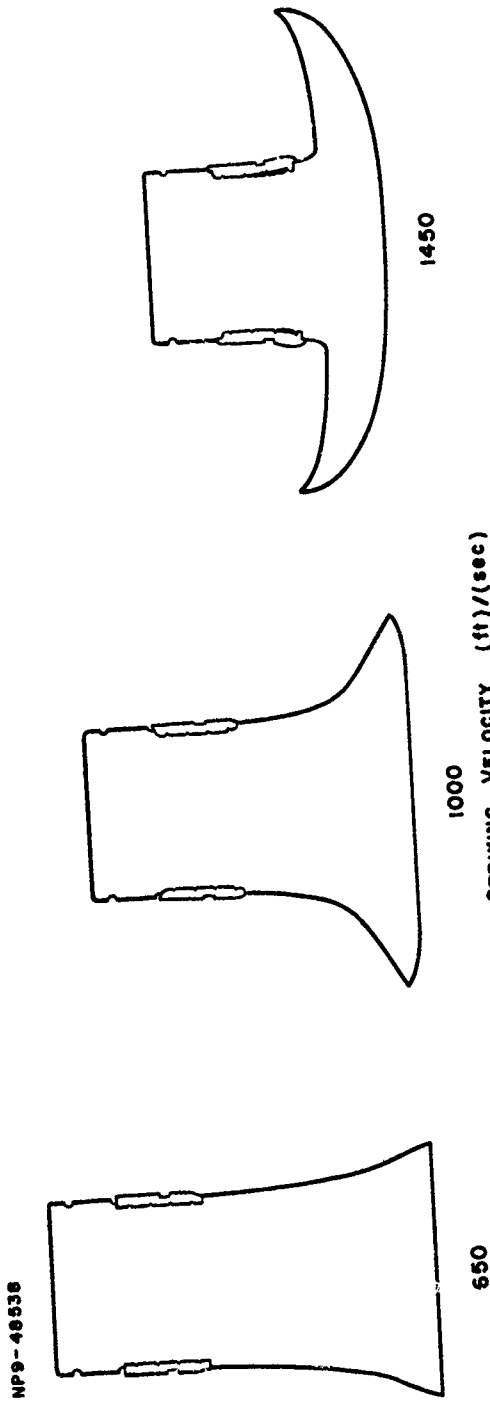


DEFORMATION CONTOURS FOR THE BALLISTIC TEST

37 mm PP Type T21 Projectile

Striking Velocity = 654 (ft)/(sec)

FIGURE (II)



PROFILES OF 37 MM PP T21 PROJECTILES AFTER IMPACT ON A FACE-HARDENED PLATE

NP9-48538

UNCLASSIFIED

NPG REPORT NO. 954

Analytical Summary Part V Plastic flow in bars and shells

DISTRIBUTION

Bureau of Ordnance:	1
Ad3	1
Re3	1
Re3a	1
Chief of Ordnance, Department of the Army Attn: ORDTX-AR	2
Commanding General, Aberdeen Proving Ground, Aberdeen, Maryland Attn: Technical Information Section Development and Proof Services	1
Commander, Operational Development Force, U. S. Atlantic Fleet, U. S. Naval Base, Norfolk 11, Virginia	1
Navy Research Section, Library of Congress, Washington 25, D. C. (Via BUORD Re3a)	2
Bureau of Ships	2
Watertown Arsenal Watertown, Mass. Attn: Armor Reports	1
Frankford Arsenal, Philadelphia, Penna.	1
Naval Ordnance Laboratory	1
Naval Ordnance Test Station, Inyokern, California Attn: Rocket Reports Attn: Research Department	1 1
Naval Research Laboratory	1
Local: OK	5
OT	1
OT-1	2
OKA-1	1
File	1

UNCLASSIFIED

SECURITY INFORMATION